THE GEOLOGICAL SOCIETY OF AMERICA®

Towards a clarification of the provenance of Cenozoic sediments in the northern Qaidam Basin

Haijian Lu[1,*], Jiacan Ye[1,2], Licheng Guo[3,4], Jiawei Pan[1], Shangfa Xiong[3,4], and Haibing Li[1]

[1]KEY LABORATORY OF DEEP-EARTH DYNAMICS OF MINISTRY OF NATURAL RESOURCES, INSTITUTE OF GEOLOGY, CHINESE ACADEMY OF GEOLOGICAL SCIENCES, BEIJING 100037, CHINA
[2]SCHOOL OF EARTH SCIENCE AND RESOURCES, CHINA UNIVERSITY OF GEOSCIENCES, BEIJING 100083, CHINA
[3]KEY LABORATORY OF CENOZOIC GEOLOGY AND ENVIRONMENT, INSTITUTE OF GEOLOGY AND GEOPHYSICS, CHINESE ACADEMY OF SCIENCES, BEIJING 100029, CHINA
[4]UNIVERSITY OF CHINESE ACADEMY OF SCIENCES, BEIJING 10049, CHINA

ABSTRACT

Determining the provenance of sedimentary basin fill in the northern Qaidam Basin is a key step toward understanding the sedimentary system dynamics and mountain-building processes of the surrounding orogenic belts in Tibet. The exceptionally thick (average of 6–8 km) Cenozoic fluvio-lacustrine deposits in the northern Qaidam Basin were once thought to have been eroded from the nearby northern Qaidam Basin margin and the southern Qilian Shan and to reflect the prolonged thrust-related exhumation of these orogenic belts. However, several recent studies, based mainly on paleocurrent and detrital zircon U-Pb age data, suggested that they were derived from the distant East Kunlun Shan to the south, or the Qimen Tagh to the southwest (at least 200 and 350 km from the northern Qaidam Basin, respectively). That model assumed that the East Kunlun Shan and Qimen Tagh formed significant topographic barriers during the earliest sedimentation of Cenozoic strata (e.g., the Lulehe Formation) in the northern Qaidam Basin. Therefore, the tectonic significance of the provenance of the Lulehe Formation remains a fundamental problem in understanding the postcollisional uplift history of the northern Tibetan Plateau. To address this issue, we conducted sedimentological and paleocurrent analyses of the Lulehe Formation and detrital zircon U-Pb dating of Mesozoic strata in the northern Qaidam Basin. The results, in combination with existing paleocurrent and seismic reflection data, collectively indicate that although the source area cannot be specified by matching zircon U-Pb ages in sedimentary rocks with crystalline basement source rocks, other evidence points consistently to a unified proximal northerly source area (the northern Qaidam Basin margin and the southern Qilian Shan). Our results emphasize that noncrystalline basement rocks (e.g., Mesozoic sedimentary rocks) in fold-and-thrust belts should be taken into consideration when seeking potential source areas by correlating zircon U-Pb ages of siliciclastic detritus with related basement rocks. In addition, this study strongly supports the claim that variations in the proportions of age populations should be used with caution when determining source terrane by comparisons of age distributions.

LITHOSPHERE; v. 11; no. 2; p. 252–272; GSA Data Repository Item 2019032 | Published online 20 December 2018 https://doi.org/10.1130/L1037.1

INTRODUCTION

In Tibet, several ranges with upthrusted basement (Gangdese, Tanggula, Kunlun, Altyn Tagh, and Qilian Shan) are separated by numerous large and small Tertiary basins trending approximately E-W to NW-SE (Liu, 1988; Pan et al., 2004; Tapponnier et al., 2001; Wang et al., 2013; Yin and Harrison, 2000; Yin, 2010). The sedimentary archives of these intermontane basins can be used to constrain the processes and mechanisms of the evolution of Tibet (Metivier et al., 1998; Yin et al., 2002). Various indicators in sedimentary basins in southern Tibet, such as the termination of marine facies sediments, the initial deposition of material derived from the Asian plate on the Indian margin, and the earliest strata to include mixed India- and Asia-sourced detritus, have been used to provide minimum constraints on the timing of the initial India-Asia collision (Garzanti et al., 1987, 1996; Najman, 2006). Sedimentologic, geochronologic, and structural analyses of Cretaceous–Tertiary basins in central Tibet have indicated multiple-phase contractional deformation since the India-Asia collision (Horton et al., 2002; Kapp et al., 2007; Li et al., 2017; Spurlin et al., 2005; Staisch et al., 2014). Further northwards, in the Qaidam Basin, there are exceptionally thick (average of 6–8 km) sequences of Cenozoic siliciclastic sediments (Rieser et al., 2006a), which have been extensively used to reconstruct depositional systems (Bush et al., 2016; Jian et al., 2013; Meng and Fang, 2008; Rieser et al., 2005; Wang et al., 2006; Zhu et al., 2006; Zhuang et al., 2011), erosional unroofing patterns (X. Cheng et al., 2016; Rieser et al., 2006a, 2006b; Wang et al., 2017; Y. Wang et al., 2015), and kinematic histories of fold-and-thrust belts and strike-slip faults along the northern, western, and southern margins of the intermontane basin (F. Cheng et al., 2016b; Fu et al., 2015; Mao et al., 2016; Meng et al., 2001; Ritts et al., 2004, 2008; Wu et al., 2012; Yin et al., 2007a, 2008a, 2008b; Yue and Liou, 1999; Yue et al., 2001; Zhang et al., 2016, 2018).

Recent integrated analyses of seismic reflection profiles and thickness distributions of Cenozoic strata across the Qaidam Basin indicated that the basin structure is predominantly a broad Cenozoic synclinorium, and hence the main depocenter lies persistently along the northwest-trending central axis of the basin (Yin et al., 2008a; Zhu et al., 2006). The spatial distribution of Cenozoic strata in the Qaidam Basin indicates that the sediments are supplied by an endorheic drainage system with sources in several ranges: in the northern basin, mainly the southern Qilian Shan (Fig. 1A); in the western basin, mainly the Altyn Tagh Range; in the southwestern basin, mainly the Altyn Tagh Range and Qimen Tagh; and in

*haijianlu2007@126.com

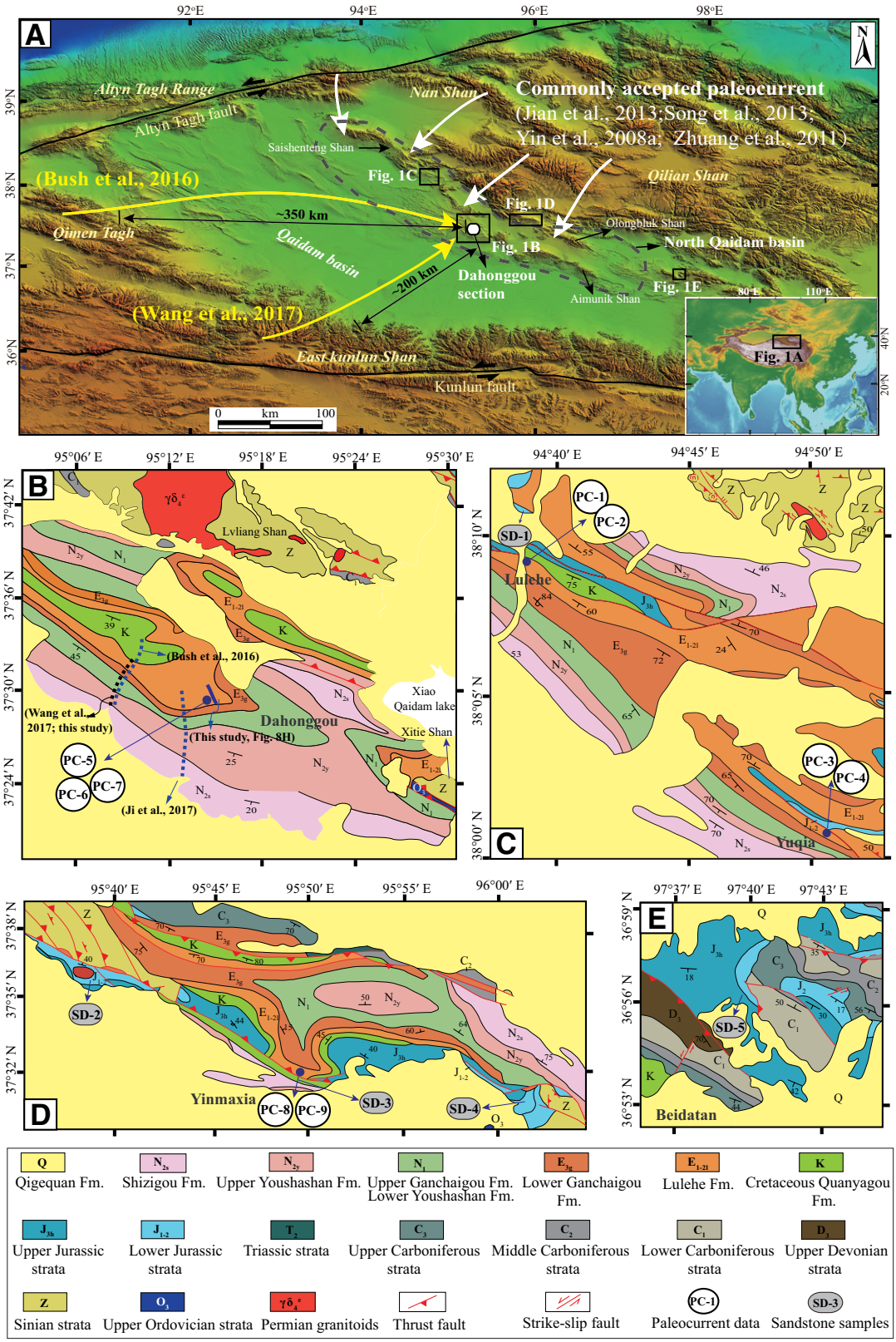

Figure 1. Location maps of the study area and sampling sites. (A) Digital elevation model (DEM) of the Qaidam Basin and adjacent orogenic belts, with schematic sediment dispersal pathways feeding the northern Qaidam Basin from three distinct perspectives. See inset map for location. The black broken line represents the approximate outline of the northern Qaidam Basin. (B–E) Geological maps of the localities of Dahonggou (B), Yuqia (C), Yinmaxia (D), and Beidatan (E), with the distributions of sampling sites.

the southern basin, mainly the East Kunlun Shan. This sediment dispersal model has been widely substantiated by paleocurrent analyses within the basin (Heermance et al., 2013; Ji et al., 2017; Jian et al., 2018; Meng and Fang, 2008; Song et al., 2013; Wu et al., 2012; Zhuang et al., 2011). However, two recent provenance studies, together with detrital zircon U-Pb and apatite fission-track dating, have challenged the widely held view by suggesting that several major paleorivers flowed across the basin axis. Specifically, Bush et al. (2016) identified E-directed paleocurrent orientations for the Lulehe Formation and the lower part of the lower Ganchaigou Formation from the Dahonggou section in the northern Qaidam Basin and suggested that the distant westernmost East Kunlun Shan (Qimen Tagh) was the principal sediment source feeding the E-directed fluvial system (Fig. 1A). Wang et al. (2017) measured NE-directed paleocurrent orientations for the Lulehe Formation and upper and lower Ganchaigou Formations from the same section and suggested that the East Kunlun Shan was the dominant provenance source (Fig. 1A), which was subsequently replaced by the southern Qilian Shan. The controversy centers on a dispute over the provenance of the Lulehe Formation strata in the northern Qaidam Basin. It is noteworthy that these two long sediment dispersal pathways require linear distances of ~200 km and ~350 km, respectively, between source and sink (Fig. 1A). These values represent only lower limits, since Cenozoic shortening strain across the Qaidam Basin has not yet been considered; notably, the magnitude of Cenozoic shortening strain increases systematically westward from ~11% in the center to ~35% in the west (Yin et al., 2008b).

It is very important to validate these discrepant provenance models, because they indicate significant topographic relief and mountain building for different orogenic belts. Most studies favoring roughly S-directed paleocurrents in the northern Qaidam Basin have linked the synorogenic coarse-grained Lulehe Formation with rapid uplift of the southern Qilian Shan at 65–50 Ma (Ji et al., 2017; Yin et al., 2008a; Zhuang et al., 2011). However, Bush et al. (2016) attributed the Lulehe Formation and the lower part of the lower Ganchaigou Formation to uplift-induced exhumation of the Qimen Tagh, whereas Wang et al. (2017) concluded that the East Kunlun Shan emerged as high relief after the deposition of the Lulehe Formation, supplying large amounts of detritus to the northern margin of the Qaidam Basin. The high-topography hypothesis for the East Kunlun Shan and Qimen Tagh during the sedimentation of the Lulehe Formation is, however, inconsistent with recent paleontological studies, which show that the Paleogene and early Neogene strata of the western Qaidam Basin contain many reefal deposits, representing lacustrine sedimentary facies (Zhong et al., 2004). The low-gradient depositional environment indicates no substantial surface uplift of the surrounding mountains.

Because the northern Qaidam Basin is a composite structure including diverse rock types produced in various ways by diverse geodynamic processes (Yang, 2002; Yin et al., 2007b), its orogenic detritus represents a variety of signatures. Unraveling the provenance of clastic wedges accumulated in the northern Qaidam Basin therefore requires sophisticated and integrated investigations. Numerous methods have been used to investigate the potential source areas of Cenozoic sedimentary rocks in the northern Qaidam Basin, including counts of conglomerate clasts (Zhuang et al., 2011), sandstone modal analysis (Bush et al., 2016; Jian et al., 2013; Rieser et al., 2005), U-Pb detrital geochronology (Bush et al., 2016; Wang et al., 2017), paleocurrent analysis (Bush et al., 2016; Ji et al., 2017; Jian et al., 2018; Song et al., 2013; Wang et al., 2017; Zhuang et al., 2011), heavy mineral analysis (Bush et al., 2016; Jian et al., 2013), $^{40}Ar/^{39}Ar$ dating of detrital white mica (Rieser et al., 2006a), and detrital apatite fission-track dating (Wang et al., 2017). Most of these methods, however, only provide indirect inferences for provenance reconstruction. For instance, Cenozoic sandstone samples within the northern Qaidam Basin exhibit a heavy mineral assemblage associated with magmatic and metamorphic basements (e.g., pyroxene, hornblende, epidote, and garnet), potentially derived from both the Kunlun Shan and Qimen Tagh and the northern Qaidam Basin margin and the southern Qilian Shan (Bush et al., 2016; Jian et al., 2013). Thus, heavy mineral analysis is not an unequivocal indicator of provenance in the northern Qaidam Basin. In addition, neither the framework grain composition of sandstones nor the geochemical composition of mudstones exhibits significant variation within the Cenozoic formations of the northern Qaidam Basin (Bush et al., 2016; Jian et al., 2013; Rieser et al., 2005). Thus, they do not enable identification of a specific source terrane. These issues are partly attributed to the orogenic recycling effect of older sedimentary units, which complicates potential provenance analyses. However, this effect has been ignored in recent studies (e.g., Wang et al., 2017).

Paleocurrent measurements can provide direct information about the orientation of the sedimentary systems and the flow directions of rivers. As a ubiquitous, chemically and physically resistant detrital mineral derived from multiple rock types, zircon is ideal for geochronological studies (Carter and Moss, 1999), and U-Pb zircon dating has been extensively used to discriminate potential sediment sources in the Tibetan Plateau (DeCelles et al., 2014; Gehrels et al., 2011; Wang et al., 2011; Wu et al., 2014; Zhuang et al., 2015). In this study, we obtained sedimentological and sedimentary petrological data from the Lulehe Formation in the Dahonggou locality, and we measured paleocurrent orientations for the Lulehe Formation at four localities; we also conducted detrital zircon U-Pb geochronologic analyses of Mesozoic sandstones from five localities in the northern Qaidam Basin. Combined with existing paleocurrent and seismic reflection data, our results strongly indicate that the provenance of the Lulehe Formation is the northern Qaidam Basin margin and the southern Qilian Shan and that the two distant sediment source models are not supported by geological observations.

GEOLOGICAL SETTING

Geography of the Qaidam Basin and Its Surroundings

Northern Tibet is characterized by several of the most prominent tectono-geomorphological features developed during the Cenozoic, including the Qilian Shan, the Altyn Tagh Range, the East Kunlun Shan, and the Qaidam Basin (Fig. 1A). These mountains have an average elevation of ~5000 m, with peaks exceeding 7000 m, whereas the intervening Qaidam Basin has an average elevation of ~2800 m, with little internal relief (Yin et al., 2007a). The transition zones between these mountains and the Qaidam Basin yield the most extensive topographic front (>500 km long) and the greatest relief (>2.5 km on average) within the plateau. The ~120,000 km^2, rhombus-shaped Qaidam Basin is tectonically bounded by the Qilian Shan–Nan Shan and northern Qaidam thrust belts to the north, the sinistral Altyn Tagh fault to the west, the Eastern Kunlun thrust belt to the south, and the dextral Wenquan fault to the east. The trend of the northern Qaidam Basin is parallel to the northern Qaidam thrust belts and the regional trend of the southern Qilian Shan. Several secondary mountain ranges are located in the northern Qaidam Basin, including, from west to east, the Saishenteng Shan, Lvliang Shan, Xitie Shan, Aimunik Shan, and Olongbluk Shan.

Bedrock Geology and Bedrock Ages

Tectono-stratigraphically, the Qilian Shan–Nan Shan region consists of three belts, composed mainly of Proterozoic shallow-marine strata in the central part sandwiched between the North Qilian complex (mainly Lower Paleozoic mélange, turbidites, and arc-type volcanic rocks) and

the South Qilian metamorphic belt (Upper Proterozoic–Lower Paleozoic metamorphic rocks; Gehrels et al., 2003a, 2003b; Yin et al., 2007b). The crystallization ages of the late Proterozoic–Mesozoic plutons are confined to two groups in the Qilian Shan and Nan Shan (Fig. 2A; Cowgill et al., 2003; Gehrels et al., 2003a, 2003b): (1) 960–920 Ma small and isolated plutons, and (2) 520–400 Ma plutons from across the entire Qilian Shan and Nan Shan. Early Paleozoic arc magmatism was contemporaneous and spatially overlapped with ultrahigh-pressure (UHP) metamorphism in the northern Qaidam Basin (Yang, 2002). The bedrock of the Eastern Kunlun Range can be subdivided into three types (Yin et al., 2007a): (1) Precambrian gneiss, Neoproterozoic metasediments, and Devonian–Carboniferous marine strata; (2) widespread Paleozoic and early Mesozoic igneous rocks (Figs. 2A and 2B); and (3) Jurassic to Cenozoic terrigenous clastics. Two main phases of plutonism are constrained to the Ordovician–Silurian and Permian–Triassic (Liu, 1988; Wu et al., 2016). The Altyn Tagh Range exposes Paleoproterozoic migmatite, gneiss, and schist, and Mesoproterozoic carbonates intruded by Proterozoic–Mesozoic granitoids (Chen et al., 2012; Cheng et al., 2017; XBGMR, 1993). The bedrock of the Qaidam Basin is composed of Precambrian–Silurian metamorphic rocks (Huang et al., 1996); in addition, one phase of prominent arc magmatism related to the subduction of the Paleo-Tethys Ocean lasted from 290–280 Ma to 215 Ma across the Kunlun-Qaidam terrane (Fig. 2C; Chen et al., 2012; Wu et al., 2016). Although the Permian–Triassic magmatism is widely exposed along the Kunlun Range, it only occurs as isolated plutons in the northern Qaidam Basin (Fig. 2B; Chen et al., 2012; Cheng et al., 2017; Wu et al., 2016). U-Pb zircon dating of granitoid samples from drill cores also testifies to the existence of a Permian–Triassic Neo-Kunlun arc in the northern and southern Qaidam Basin (Fig. 2B; Cheng et al., 2017). The earliest phase (2.5–2.3 Ga) of magmatism was identified in the Quanji Massif, in the northern Qaidam Basin (C. Wang et al., 2015).

Mesozoic–Cenozoic Strata in the Northern Qaidam Basin

Besides the early Paleozoic UHP metamorphic gneiss in the Lvliang Shan, Xitie Shan, and Dulan areas along a 450-km-long belt in the northern Qaidam Basin (Yang, 2002; Yin et al., 2007b), Jurassic and Cretaceous sedimentary rocks crop out discontinuously along the margin of the northern Qaidam Basin from Lenghu to Dameigou (Figs. 1 and 2; Ritts and Biffi, 2001; Yu et al., 2017). The ages of Mesozoic strata have been determined predominantly by paleontological studies and lithostratigraphic correlation (Ritts and Biffi, 2001, and references therein). Jurassic and Cretaceous strata are entirely nonmarine, nonvolcanogenic sedimentary rocks, and their lithology grades from boulder conglomerates to laminated shales (Ritts and Biffi, 2001). The depositional environments of these sedimentary rocks ranged from alluvial fans through coarse- and fine-grained fluvial systems, to deep, open lakes (Ritts and Biffi, 2001). Detrital zircon age data indicate that the Jurassic sedimentary rocks have two major age peaks of ca. 250 Ma and ca. 2400 Ma, and two minor peaks of ca. 450 Ma and ca. 850 Ma (Yu et al., 2017). This age distribution pattern is similar to that of the East Kunlun Range, which may complicate potential provenance analyses of Cenozoic strata in the northern Qaidam Basin. The inferred tectonic setting of Mesozoic rocks on the margin of northern Qaidam Basin remains disputed, with most researchers arguing for a predominantly extensional setting (Chen et al., 2003; Wu et al., 2011; Xia et al., 2001; Yu et al., 2017), and a few for a compressional setting (e.g., Ritts and Biffi, 2001). The provenance of these strata is also highly controversial, with one view arguing for the Qilian Shan (Ritts and Biffi, 2001) and the other for the East Kunlun Shan (Yu et al., 2017).

Cenozoic deposits with a maximum thickness of 12,000 m and an average thickness of 6–8 km are widely distributed across the Qaidam Basin. Seismic reflection data indicate that the Qaidam Basin is a broad Cenozoic synclinorium with its depocenter located persistently along the northwest-trending central axis of the basin (Meng and Fang, 2008; Yin et al., 2008a; Zhu et al., 2006). The depocenter has shifted progressively southeastward during the Cenozoic, from an initial position in the northwestern basin to its current depocenter at Dabuxun Lake near the basin center (Yin et al., 2008a; Zhu et al., 2006). A composite structural model was proposed to account for the spatio-temporal evolution of the sedimentary architecture in the Qaidam Basin, including south-directed thrusts carrying the low-elevation Qaidam Basin over the high-elevation Eastern Kunlun Range along the southern margin of the basin and crustal-scale triangular zones tapering from the northern margin toward the basin interior (Yin et al., 2007a, 2008a, 2008b). This model may also explain the observations that, whereas pre-Quaternary basin fills are widely exposed in the northern Qaidam Basin, they are rare in the southern Qaidam Basin. Traditional provenance analyses of sandstone petrography, heavy minerals, paleocurrents, and conglomerate counts usually indicate that Cenozoic sediments adjacent to basin margins are directly linked to the adjacent mountain belts (Hanson, 1999; Jian et al., 2013; Wu et al., 2012; Zhuang et al., 2011).

Cenozoic outcrops are thickest in the Dahonggou and Lulehe localities in the northern Qaidam Basin (QBGMR, 1984), and they show an initial upward-fining and then an upward-coarsening trend (Bush et al., 2016; Fang et al., 2007; Ji et al., 2017; Lu and Xiong, 2009; Wang et al., 2017). This exceptionally thick succession has been divided into seven formations, including, in ascending order, Qigequan, Shizigou, upper Youshashan, lower Youshashan, upper Ganchaigou, lower Ganchaigou, and Lulehe. The Lulehe Formation at the Dahonggou section consists of poorly sorted, clast-supported, granule-cobble conglomerates interbedded with medium- to coarse-grained, trough cross-stratified sandstones representing an alluvial-fan and braided fluvial system. The lower Ganchaigou Formation is dominated by interbedded sandstone, or siltstone and mudrock deposits, and it represents a fine-grained fluvial system. The upper Ganchaigou Formation is predominantly composed of the interbeds of laminated or massive mudstones and ripple-laminated siltstones and likely also represents a fine-grained fluvial system. The lower Youshashan Formation consists of alternating brown laminated or bedded mudstone and gray-green massive sandstone, or conglomerate, or siltstone, and it represents a coarse-grained fluvial system. The upper Youshashan Formation is mostly composed of interbedded conglomerate and sandy conglomerate, with brown or yellow massive sandstone intercalated with yellow massive siltstone, and it represents a sandy to gravelly braided fluvial system. The Shizigou Formation consists of coarse-grained conglomerate and medium- to very coarse-grained sandstone, representing a sandy to gravelly braided fluvial or alluvial-fan system. The horizontal Qigequan Formation unconformably overlies the Shizigou Formation and consists of conglomerate, sandy conglomerate, sandstone, and siltstone deposits. Typically, the stratigraphic ages of the Qaidam Basin sediments are bracketed between the Paleocene–Eocene and Quaternary (Chang et al., 2015; Fang et al., 2007; Ji et al., 2017; Lu and Xiong, 2009; Sun et al., 2005). Recently, however, this long-held view was challenged by a new magnetostratigraphic study of the Dahonggou section, bolstered by newly discovered mammalian fossils (Wang et al., 2017). The latter suggested a far younger basal age of ca. 25 Ma for the Lulehe Formation.

SAMPLING AND ANALYTICAL METHODS

Paleocurrent Analyses

Paleocurrent directions were measured from fluvial and alluvial strata of the Lulehe Formation in the northern Qaidam Basin, using

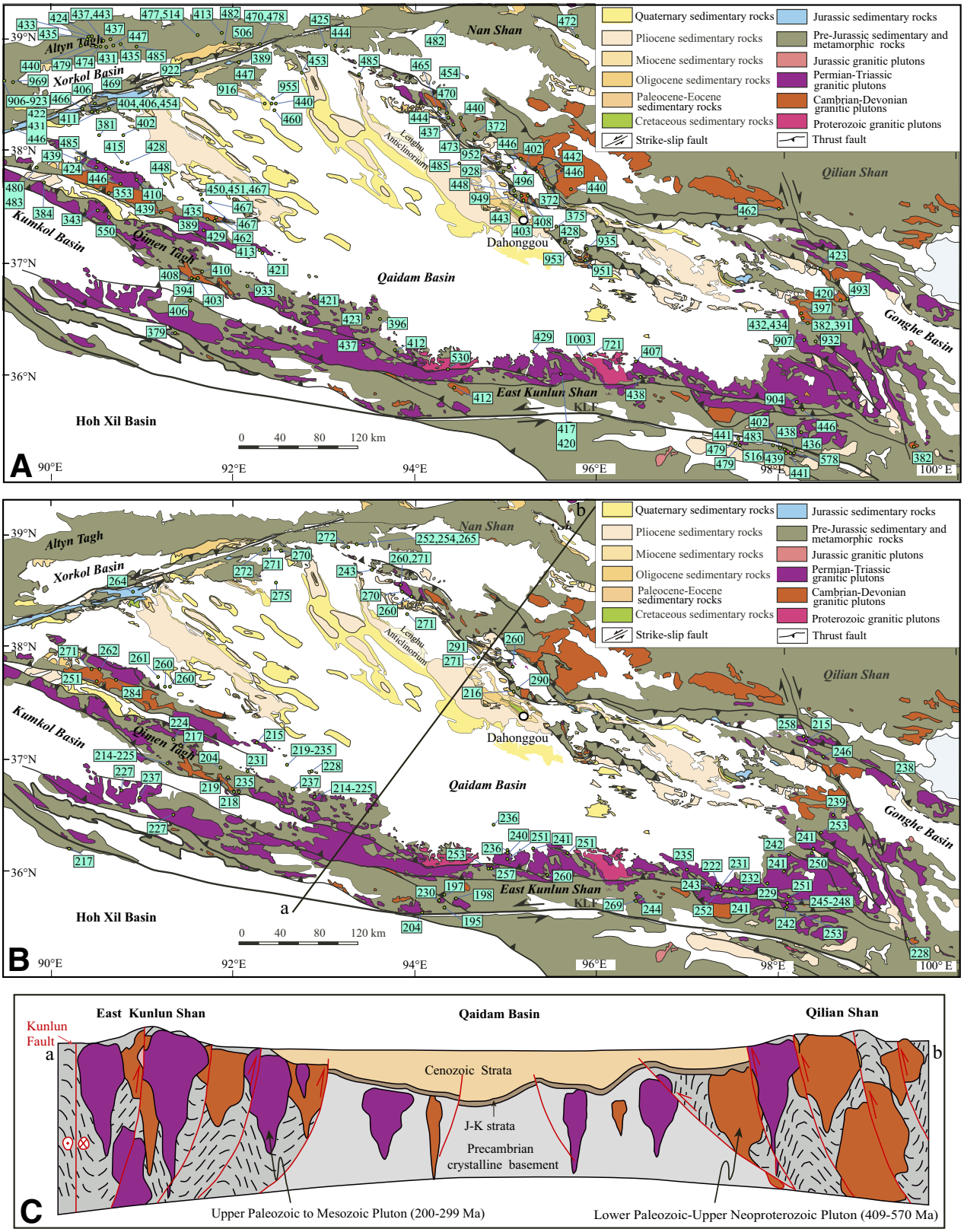

Figure 2. Zircon U-Pb age data and subsurface structure of the Qaidam Basin and surrounding mountains, adapted from Cheng et al. (2017). Geological map of the Qaidam Basin and surrounding mountains is modified from Bush et al. (2016), with zircon ages for Proterozoic–early Paleozoic plutons (A) and for Permian–Triassic plutons (B). Note that several Permian–Triassic ages superimposed on Quaternary unconsolidated sediments (white) are based on drill-core data (Cheng et al., 2017). (C) Schematic cross section of a transect (a–b) extending from the East Kunlun Shan northeastwards to the Qilian Shan. See part B for location. J-K—Jurassic–Cretaceous; KLF—Kunlun Fault.

cross-stratification (eight measurements at one station) and pebble-cobble imbrication (517 measurements at eight stations), in the localities of Lulehe, Yuqia, Dahonggou, and Yinmaxia (Fig. 3). The Dahonggou locality is ~5 km east of the previous section of Bush et al. (2016) and Wang et al. (2017). The dip direction and dip angle of planar paleocurrent indicators (cross-strata, pebble-cobble imbrication) were measured in the field with a Brunton compass. We measured 62 and 42 pebble-cobble imbrications in two horizons at the Lulehe locality. Two layers with 93 and 59 pebble-cobble imbrications were recorded at the Yuqia locality, and two horizons with 50 and 50 pebble-cobble imbrications, plus one horizon with eight cross-strata data, were measured at the Dahonggou locality. Finally, we measured 56 and 105 pebble-cobble imbrications in two layers at the Yinmaxia locality. Detailed global positioning system (GPS) locations of all measuring points and attitudes (dip directions and dip angles) of all the pebble-cobble imbrications and cross-beddings are listed in the GSA Data Repository Table DR1.[1] Structural restoration of the paleocurrent data was accomplished using a stereonet computer program.

Zircon U-Pb Dating

Five unweathered medium-grained Jurassic–Cretaceous sandstone samples were collected from five localities in the northern Qaidam Basin (Figs. 1C–1E). We attempted to minimize the effects of weathering by excavating and collecting the freshest samples possible. For each sample, an ~5 kg aliquot of medium-grained sandstone was collected and processed according to standard mineral separation techniques. Subsequently, ~250 zircon grains were randomly mounted in epoxy resin and then polished to obtain a smooth flat internal surface. Reflected and transmitted light microscopy, as well as cathodoluminescence (CL) imagery, was used to identify ideal grains for U-Pb analysis. Approximately 100 zircon grains were randomly selected for analysis using laser ablation–multicollector–inductively coupled plasma–mass spectrometry (LA-MC-ICP-MS) at the Key Laboratory of Continental Tectonics and Dynamics, Institute of Geology, Chinese Academy of Geological Sciences, Beijing, China. Analyses were conducted using a laser spot size of 32 mm and a repetition rate of 5 Hz under 70% energy conditions, and with a 91500 zircon standard for calibration. Detailed methods have been described in Yuan et al. (2004).

RESULTS

Paleocurrent Directions

The results of paleocurrent analyses are reported in Table DR1, and a rose diagram is illustrated in Figure 4. Two horizons at the Lulehe locality display a consistent NE-directed flow for the Lulehe Formation deposits. Given the occurrence of coarse-grained boulders at the Lulehe section, the results most likely reflect a high-energy depositional system and proximal sediment source. Therefore, we attribute the two NE-directed paleoflow directions to thrust-related exhumation of the Saishenteng Shan, immediately west of the Lulehe section. Two horizons at the Yuqia locality show a consistent SE-directed flow for the Lulehe Formation. The paleocurrents indicated by the Lulehe Formation at the Dahonggou locality flow SW, and then SE, whereas those indicated by the Lulehe Formation at the Yinmaxia locality flow consistently SW.

Detrital Zircon Ages

Representative CL images of detrital zircon grains from the five sandstone samples are displayed in Figure 5, and the analytical data are listed in Table DR2. It is generally acknowledged that younger $^{206}Pb/^{238}U$ ages (younger than 1000 Ma) are often more precise, whereas older $^{206}Pb/^{207}Pb$ ages (older than 1000 Ma) are often more precise (Gehrels et al., 2011). Provenance determinations were based mainly on age clusters that included at least three analyses (Gehrels et al., 2011). Major age groups and their corresponding peak ages were evaluated by visual inspection of the detrital zircon U-Pb age probability plots for all five samples (Fig. 6A). In this study, the major peak refers to age populations having more than 30% of the total number of data, whereas minor peaks refer to those with less than 20%. A total of 500 detrital zircon grains produced data of sufficient precision for geochronological interpretation (Fig. 6A).

The zircon grains of Early Jurassic sample SD-1 exhibited both euhedral and abraded shapes, with sizes ranging from 50 to 200 μm (Fig. 5). The crystals displayed half distinct oscillatory and half faint zoning on CL images, suggesting both magmatic and metamorphic origins. The Th/U ratios varied from 0.01 to 3.23. Detrital zircon grains of sample SD-1 are 260–2830 Ma in age, with one major peak at 850 Ma and several minor peaks at 266, 463, 1820, and 2451 Ma. The zircon grains of Early Jurassic sample SD-2 showed both euhedral and abraded shapes, with sizes ranging from 50 to 300 μm (Fig. 5). Most of the crystals (~70%) displayed faint zoning on CL images, but the rest of the crystals showed distinct oscillatory zoning. The Th/U ratios ranged from 0.01 to 3.03. The age-distribution diagram of sample SD-2 shows one major peak at 446 Ma and two subordinate peaks at 240–292 and 952 Ma. The zircon grains of Cretaceous sample SD-3 showed both euhedral and abraded shapes, with sizes ranging from 50 to 300 μm (Fig. 5). Most of the crystals (~60%) displayed faint zoning on CL images, but the rest showed distinct oscillatory zoning. The Th/U ratios ranged from 0.01 to 3.69. The sample has a unimodal distribution, with one major peak at 460 Ma and rare Paleoproterozoic and Neoproterozoic grains. The zircon grains of sample SD-4 showed both euhedral and abraded shapes, with sizes ranging from 60 to 280 μm (Fig. 5). Most of the crystals (~70%) displayed faint zoning on CL images, and the rest showed distinct oscillatory zoning. The Th/U ratios ranged from 0.04 to 3.81. The sample yielded a unimodal Paleoproterozoic peak of 2452 Ma, which is consistent with other age results for the same section (Qian et al., 2018; Yu et al., 2017). The zircon grains of sample SD-5 showed both euhedral and abraded shapes, with sizes ranging from 60 to 200 μm (Fig. 5). Most of the crystals (~60%) displayed faint zoning on CL images, but the rest showed distinct oscillatory zoning. The Th/U ratios ranged from 0.17 to 3.76. The sample exhibited diverse zircon age spectra, with one major peak at 449 Ma and two minor peaks at 983 and 2503 Ma.

CORRECTION OF THE STRATA

Calculation errors and differences in the boundaries assigned to each formation by different researchers may result in differences in the thickness of each formation at the same section. Several studies previously measured the thickness of the Lulehe Formation at the Dahonggou locality (Fig. 1B), and most of them obtained a relatively consistent thickness of 386–490 m (Zhuang et al., 2011; Ji et al., 2017; Wang et al., 2017). Our investigations in the field yield a thickness of ~546 m for the Lulehe Formation at the eastern Dahonggou section (Fig. 1B). This slight inconsistency is due to different boundary assignments for the Lulehe Formation. However, Bush et al. (2016) reported a thickness of 1100 m for the Lulehe Formation, which is more than twice that of other estimates. After careful examination, we discovered that Bush et al. (2016)

[1] GSA Data Repository Item 2019032, Table DR1: Paleocurrent measurements of the Lulehe Formation deposits in northern Qaidam Basin, and Table DR2: Detrital zircon U-Pb ages of Mesozoic sandstone samples from the northern Qaidam Basin margin, is available at http://www.geosociety.org/datarepository/2019, or on request from editing@geosociety.org.

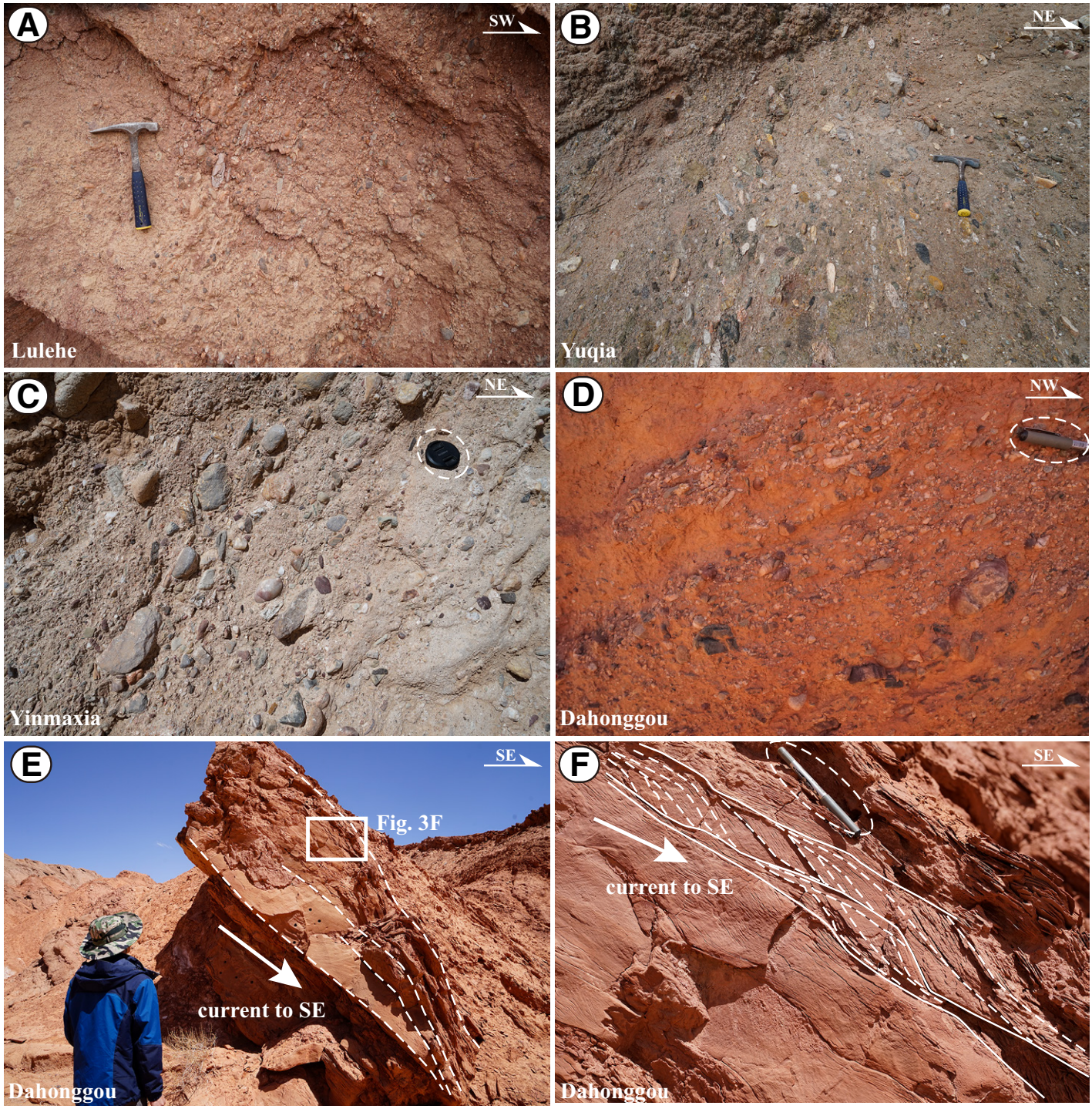

Figure 3. Primary sedimentary structures of the Lulehe Formation, including pebble imbrication (A–D) and ripple marks in wedge-shaped cross-stratification (E–F), used for paleocurrent measurement at the localities of Lulehe, Yuqia, Yinmaxia, and Dahonggou in the northern Qaidam Basin.

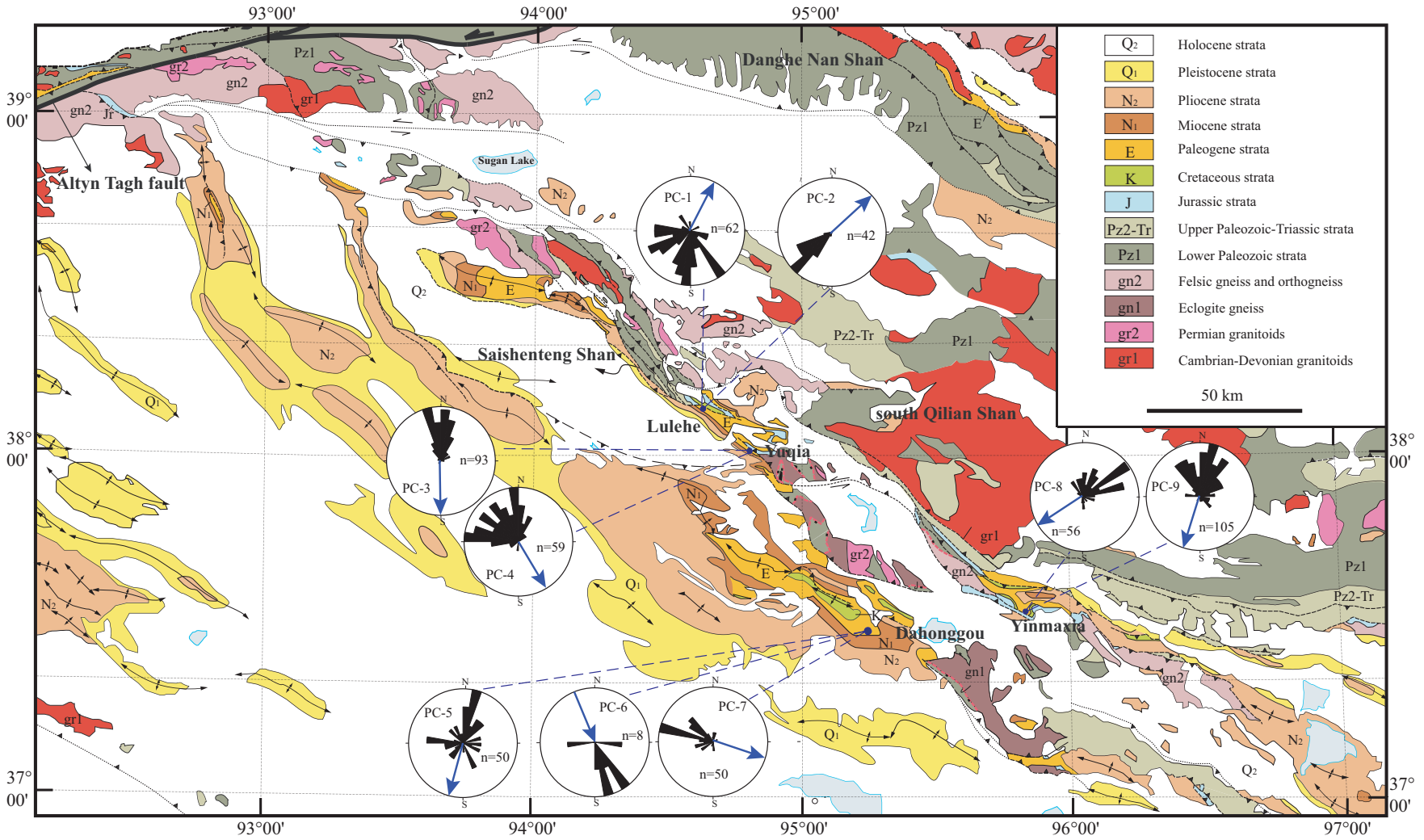

Figure 4. Regional geological map of the northern Qaidam Basin and the southern Qilian Shan with paleocurrent directions plotted on rose diagrams for the Lulehe Formation deposits, adapted from Yin et al. (2008a). Blue arrows represent mean paleocurrent vector within individual intervals; *n*—number of measurements.

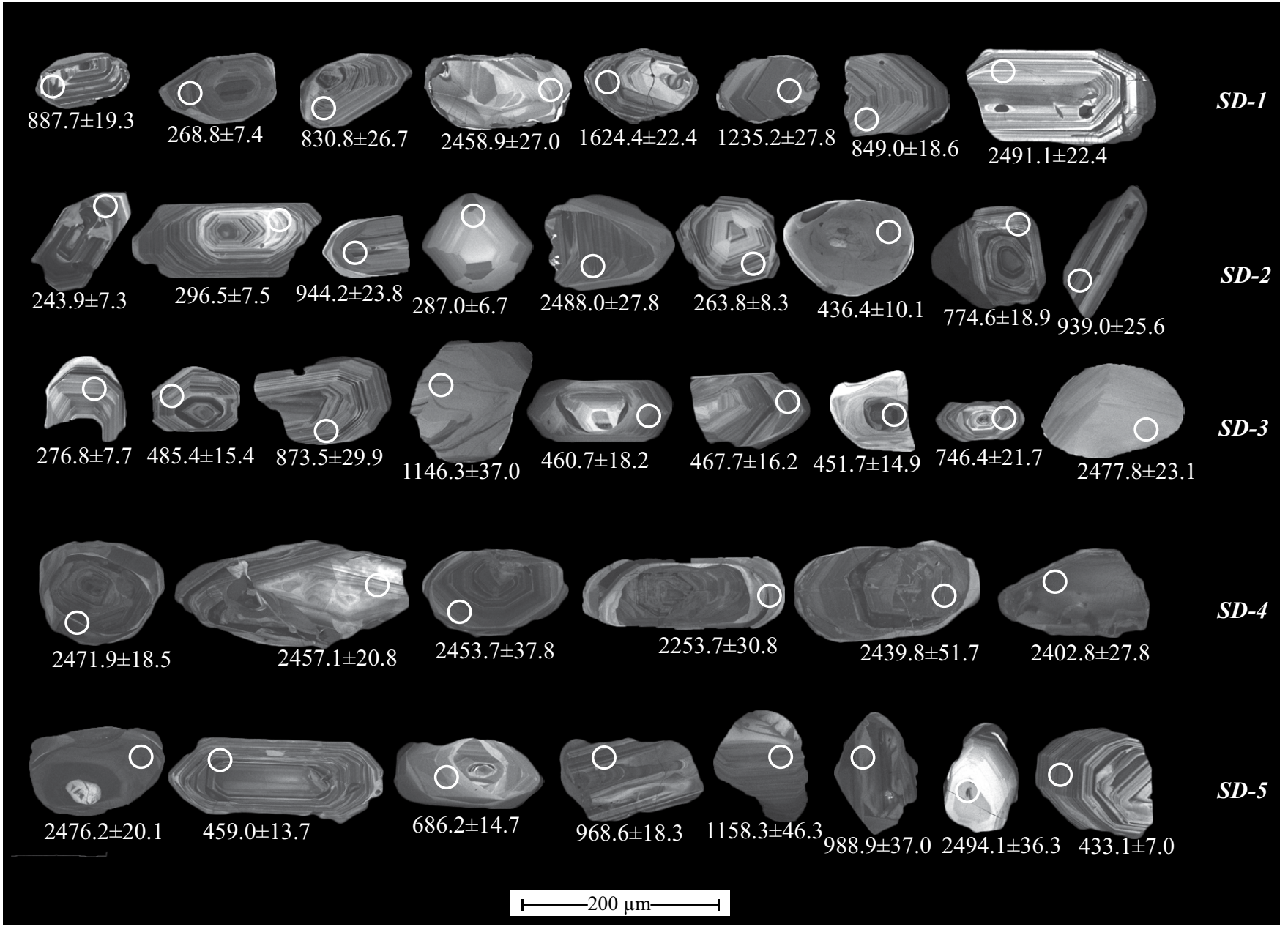

Figure 5. Representative cathodoluminescence (CL) images of detrital zircon grains from five sandstone samples. White circles indicate the locations of U-Pb analysis spots. Numbers are U-Pb ages in Ma with 1σ uncertainty.

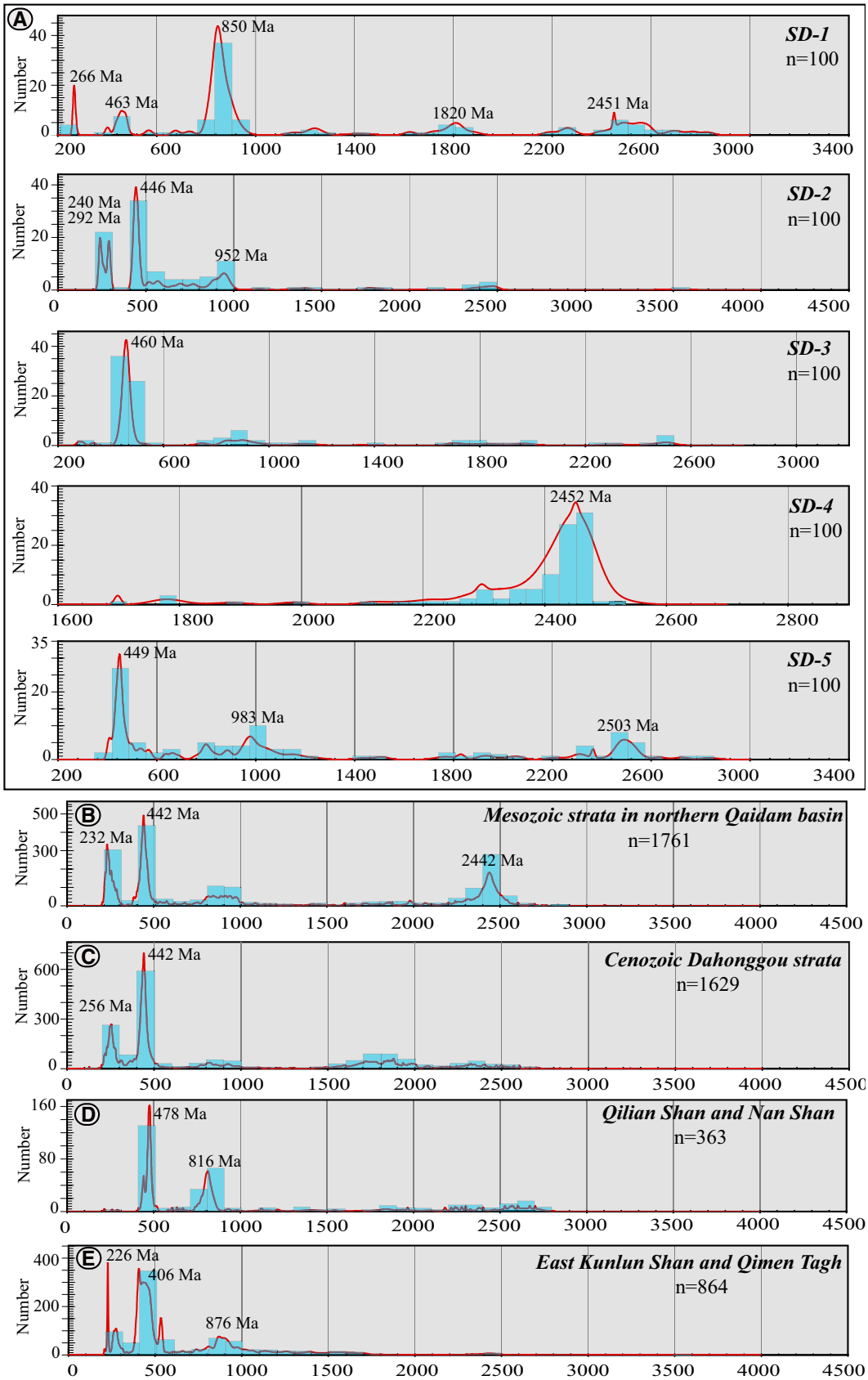

Figure 6. Probability distribution diagrams of zircon ages from different geological units. (A) Five Mesozoic sandstone samples from the northern Qaidam Basin (this study). (B) Mesozoic strata from the northern Qaidam Basin (Yu et al., 2017; Bush et al., 2016; this study). (C) Cenozoic Dahonggou strata from the northern Qaidam Basin (Bush et al., 2016; Wang et al., 2017). (D) Qilian Shan and Nan Shan (Chen et al., 2012; Gehrels et al., 2003a, 2011; Menold et al., 2009). (E) East Kunlun Shan and Qimen Tagh (He et al., 2016; Li et al., 2013; Xia et al., 2015).

misidentified the underlying Cretaceous Quanyagou Formation as the lower part of the Lulehe Formation (Fig. 1B). There is an unconformable contact between the Quanyagou and Lulehe Formation (QBGMR, 1984), but the poor exposure of the Quanyagou and Lulehe Formation at the western section, likely the result of intensive weathering and erosion caused by underground springs, may blur the boundary between the Quanyagou and Lulehe Formation. The near-indistinguishable boundary of the two formations may have led to this error.

Bush et al. (2016) collected samples for detrital zircon U-Pb geochronology and paleocurrent analysis at the Dahonggou section to determine provenance (Fig. 1B). Through strata correction, we are certain that four samples for zircon U-Pb dating and five horizons for paleocurrent analyses from the lower part of the Lulehe Formation were in fact collected from the Cretaceous Quanyagou Formation (QBGMR, 1984). Provenance analyses of the Cretaceous Quanyagou Formation indicated that large amounts of clastic materials from the western Kunlun Shan (Qimen Tagh) were transported to the Dahonggou section by an E-directed axial fluvial system (Bush et al., 2016). However, this view is inconsistent with previous provenance analyses of Cretaceous strata in the northern Qaidam Basin margin, which suggested the derivation of siliciclastic detritus from the Qilian Shan (Ritts and Biffi, 2001). However, discussion of the provenance of Cretaceous strata is beyond the scope of the present study. To compare the provenance results of Cenozoic strata from different studies, we excluded the detrital zircon U-Pb geochronology and paleocurrent data from the Cretaceous Quanyagou Formation (Bush et al., 2016) in the following discussion.

SEDIMENTOLOGY OF THE LULEHE FORMATION

The Lulehe Formation is named for its type section at the Lulehe locality (QBGMR, 1980). It is widely exposed within the northern Qaidam Basin, where four localities were investigated in this study (Figs. 1 and 7). Typically, the Lulehe Formation unconformably overlies Mesozoic strata and conformably underlies the lower Ganchaigou Formation and is composed of terrigenous clastic red beds (Figs. 7 and 8) with a thickness of 400–500 m (Zhuang et al., 2011; Ji et al., 2017; Wang et al., 2017). The division between the Lulehe Formation and the lower Ganchaigou Formation is easily determined by the presence and absence of sandy and conglomeratic red beds, respectively. The Lulehe Formation deposits contain large amounts of cobble-boulder conglomerates (Fig. 7) and are usually interpreted as a synorogenic coarse-grained conglomerate deposited by high-gradient depositional systems (Zhuang et al., 2011; Ji et al., 2017; Yin et al., 2008a). The depositional environments of the Lulehe Formation can be reconstructed based on sedimentological observations of the 546-m-thick measured stratigraphic interval of the eastern Dahonggou section (Fig. 1B).

The Lulehe Formation at the Dahonggou section is divisible into two parts based on lithofacies assemblages and lithological characteristics. The lower part of the section (0–284 m) is characterized by a diverse

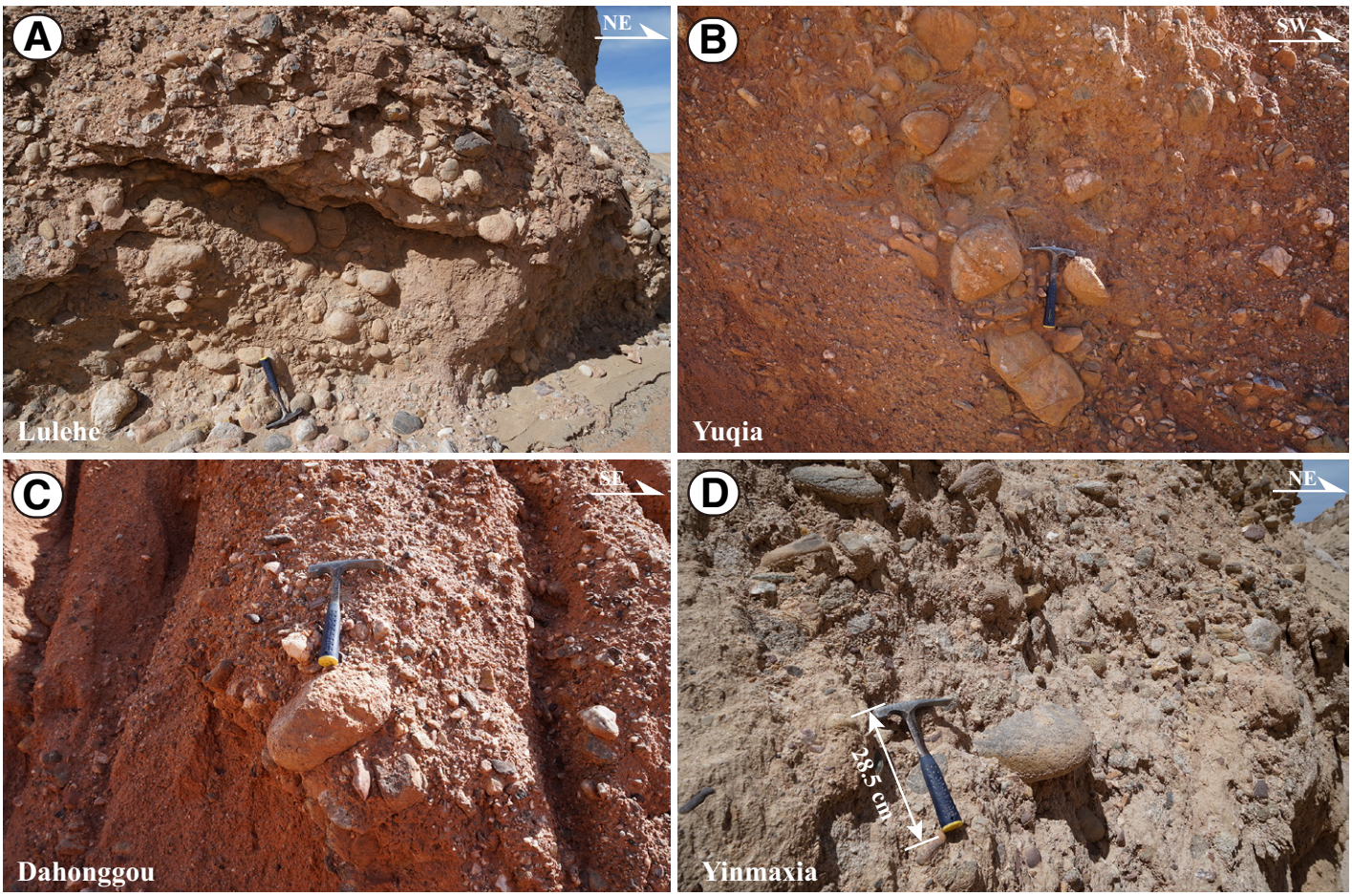

Figure 7. Abundant cobble-boulder conglomerates (mainly Gcm, Gmm, and Gcmi) in the lower part of the Lulehe Formation at the localities of Lulehe, Yuqia, Dahonggou, and Yinmaxia in the northern Qaidam Basin. See Table 1 for lithofacies codes.

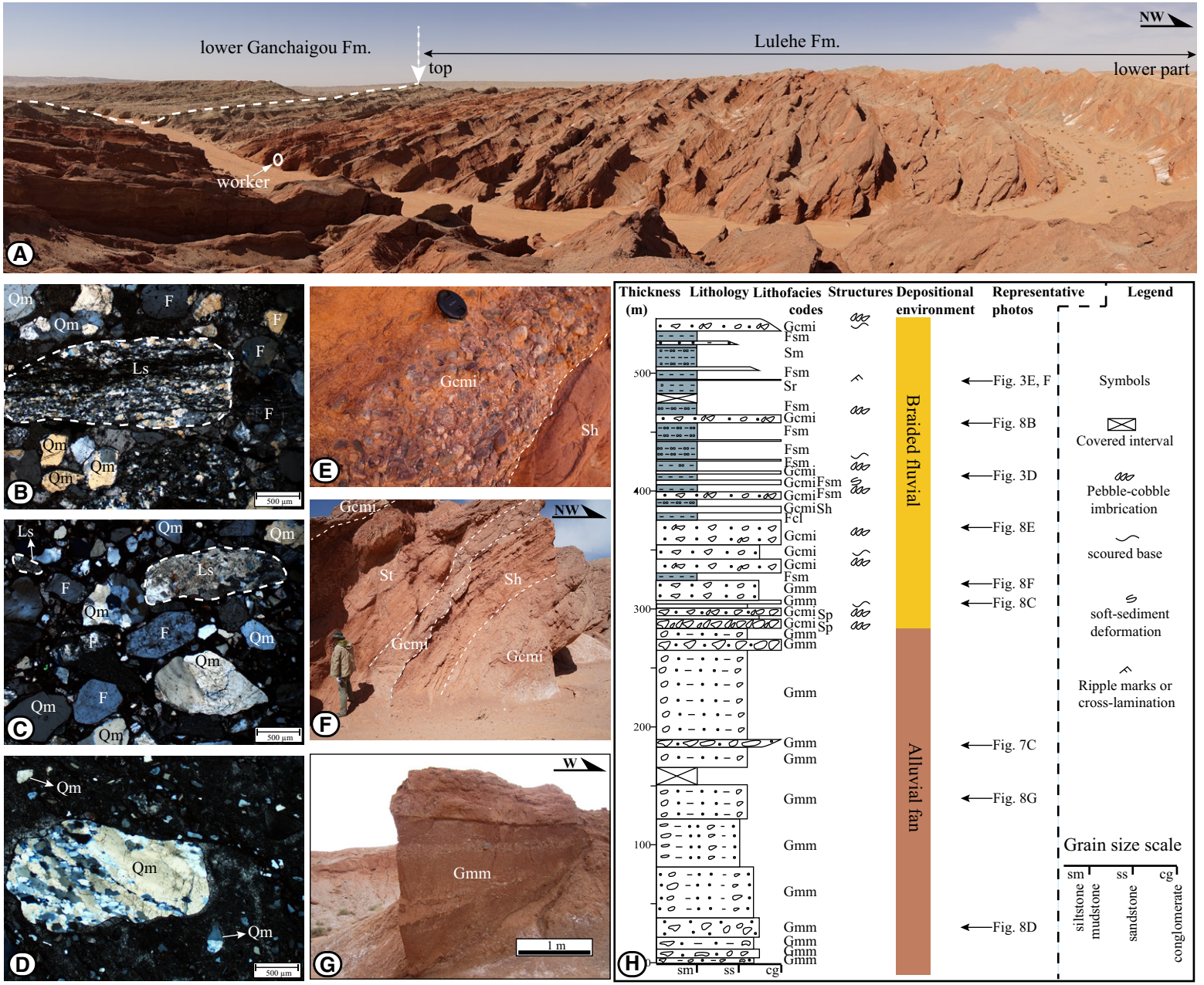

Figure 8. Measured stratigraphic section of the Lulehe Formation at the Dahonggou locality. (A) Excellent outcrop of the Lulehe Formation dominated by sandy and conglomeratic red beds. (B–D) Photomicrographs of feldspatholithic (B–C) and quartz-arenitic (D) petrofacies. The two feldspatholithic sandstones contain feldspar (F) and sedimentary lithic (Ls) grains, in addition to monocrystalline quartz (Qm); the quartzose example consists of 100% monocrystalline quartz (mainly Qm) grains. See part H for locations. (E–F) Interbeds of clast-supported pebble-cobble conglomerate and red siltstone, with a sharp, erosive contact, in the upper part of the Lulehe Formation. (G) Massive, matrix-supported and poorly sorted, pebble to boulder conglomerates in the lower part of the Lulehe Formation. (H) Vertical succession of lithofacies and depositional system of the measured section. See Table 1 for lithofacies codes.

assemblage of poorly sorted, matrix-supported pebble-boulder conglomerates (mainly Gcm, Gmm, and Gcmi) mixed with brick-red mudstones, siltstones, and sandstones with mottling (Fig. 8G). Beds are usually more than 2 m thick, and occasionally exceed 40 m. The pebble to boulder conglomerates are composed of clasts derived from local basement lithologies (granitoid intrusive rocks, metamorphic rocks, and sedimentary rocks; Zhuang et al., 2011). The sandstones of this unit are texturally immature and matrix-supported, with poor sorting and grain sizes up to granular and pebbly sand (Fig. 8D). However, the sandstones, predominantly composed of monocrystalline quartz, are compositionally hypermature, reflecting derivation from a stable, deeply weathered source area or orogenic recycling of quartzose sedimentary rocks (DeCelles et al., 2014). The texturally immature, compositionally mature aspect of the sandstones in the lower part of the Lulehe Formation indicates that the sediments were derived from a highly weathered terrane and were transported rapidly from source to sink by concentrated density flows (DeCelles et al., 2014). We interpret this sequence to represent debris-flow deposition on an alluvial fan or on fan-delta slopes (Table 1; Miall, 1978; DeCelles et al., 1991).

A distinguishing feature of the upper part of the section (284–546 m) is the presence of moderately sorted, clast-supported, unstratified, imbricated pebble to cobble conglomerates (mainly Gmm and Gcmi) alternating with brick-red siltstones, sandstones, and mudstones (Figs. 8A, 8E, and 8F). These deposits have an erosive and sharp boundary (Figs. 8E and 8F). The conglomerate beds are usually 0.5–5 m thick, and the interbedded sandstones, siltstones, or mudstones are 0.5–10 m thick. The unit is characterized by normal-graded bedding, climbing ripple laminations, parallel bedding, soft-sediment deformation, and trough cross-stratification (Fig. 8H). The sandstones are subangular to subrounded and moderately sorted (Figs. 8B and 8C). The sandstone compositions fall into the feldspatholithic group (McBride, 1963), based on the presence of large amounts of feldspar and sedimentary lithic grains (Figs. 8B and 8C). In contrast to the lower part of the Lulehe Formation, the sandstones of the upper part have submature textures and immature compositions. The abundance of feldspar and sedimentary lithic grains indicates the presence of sedimentary rocks in the source terrane. Based on these observations, we interpret the sequence to represent braided-fluvial deposits (Table 1; Miall, 1978; DeCelles et al., 1991).

PROVENANCE INTERPRETATION

Our field observations, together with sedimentological, paleocurrent, and detrital zircon U-Pb age data, substantially improve our understanding of the tectono-sedimentary evolution of the Cenozoic strata in the northern Qaidam Basin. Comparison of detrital zircon U-Pb ages between the Dahonggou sedimentary rocks and potential sources (the northern Qaidam Basin margin and the southern Qilian Shan, East Kunlun Shan, and Qimen Tagh), in conjunction with sedimentology, paleocurrent, seismic reflection data, helps to determine the prime candidate for the source region of the Dahonggou section: the northern Qaidam Basin margin and the southern Qilian Shan or the East Kunlun Shan and Qimen Tagh.

Sedimentological and Stratigraphic Evidence

Sedimentological analyses indicate that the strata of the Lulehe Formation at the Dahonggou locality are dominated by conglomeratic and sandy brick-red beds and were deposited initially in an alluvial fan and subsequently in a braided-fluvial system. This conclusion is broadly consistent with previous studies at the localities of Dahonggou (Ji et al., 2017; Song et al., 2013; Bush et al., 2016; Zhuang et al., 2011), Mahai (Zhuang et al., 2011), or Lulehe (Zhuang et al., 2011), which indicated that the deposits of the Lulehe Formation represent a high-gradient depositional system and synorogenic sedimentation, suggestive of a proximal uplifted source terrane (e.g., the northern Qaidam Basin margin and the southern Qilian Shan). Photomicrographs of the Lulehe Formation sandstones reveal the presence of large amounts of unstable feldspar and sedimentary lithic grains (Figs. 8B and 8C), which have also been identified in previous sedimentary petrological studies at Lulehe, or at other localities in the Qaidam Basin (F. Cheng et al., 2016a; Fu et al., 2013; Jian et al., 2013). Presumably, the source area was uplifted and eroded so rapidly that there was insufficient time for physical weathering of the feldspar and sedimentary lithic grains. These results demonstrate the significant derivation of sedimentary rocks from a proximal source terrane (e.g., Mesozoic sedimentary rocks in the northern Qaidam Basin margin), which has important implications for identifying potential source terranes based on detrital zircon U-Pb geochronology, as discussed below.

According to previous studies, continental red beds typically develop as alluvial fan and fluvial deposits and are the earliest deposits associated with the onset of compressive deformation, and they are assumed to represent the initiation of syntectonic sedimentation (Turner, 1980). They have been regarded as clastic wedges of sediment formed along the flanks of actively rising mountain regions, implying strong tectonic control in the form of marginal faulting and uplift of the source regions (Turner, 1980). Interestingly, this wedge-shaped structure was identified

TABLE 1. LITHOFACIES AND INTERPRETATIONS USED IN THIS STUDY

Lithofacies code	Description	Interpretation
Fsm	Massive, bioturbated, mottled siltstone, usually red; carbonate nodules common	Paleosols, usually calcic or vertic
Sm	Massive medium- to fine-grained sandstone; bioturbated	Bioturbated or pedoturbated sand, penecontemporaneous deformation
Sr	Fine- to medium-grained sandstone with small, asymmetric, two- and three-dimensional current ripples	Migration of small two-dimensional (2-D) and three-dimensional (3-D) ripples under weak (~20–40 cm/s), unidirectional flows in shallow channels
St	Medium- to very coarse-grained sandstone with trough cross-stratification	Migration of large 3-D ripples (dunes) under moderately powerful (40–100 cm/s), unidirectional flows in large channels
Sp	Medium- to very coarse-grained sandstone with planar cross-stratification	Migration of large 2-D ripples under moderately powerful (~40–60 cm/s), unidirectional channelized flows; migration of sandy transverse bars
Sh	Fine- to medium-grained sandstone with plane-parallel lamination	Upper plane bed conditions under unidirectional flows, either strong (>100 cm/s) or very shallow
Gcm	Pebble to boulder conglomerate, poorly sorted, clast-supported, unstratified, poorly organized	Deposition from sheetfloods and clast-rich debris flows
Gcmi	Pebble to cobble conglomerate, moderately sorted, clast-supported, unstratified, imbricated (long axis transverse to paleoflow)	Deposition by traction currents in unsteady fluvial flows
Gmm	Massive, matrix-supported pebble to boulder conglomerate, poorly sorted, disorganized, unstratified	Deposition by cohesive mud-matrix debris flows

Note: Modified after Miall (1978) and DeCelles et al. (1991).

by seismic reflection profiling in the Qaidam Basin (Cheng et al., 2017; Wei et al., 2016; Yin et al., 2008b). The Lulehe Formation deposits in sections A–B and C–D of Figure 9 are thickest in the northern Qaidam Basin margin; they then thin to the southwest and then disappear before reaching the basin center (Yin et al., 2008b; Wei et al., 2016). A transverse section (E–F) along the central axis of the basin also supports the absence of the Lulehe Formation deposits at the center of Qaidam Basin, south of the Dahonggou section (Fig. 9D; Cheng et al., 2017). These findings are consistent with an isopach map of the Lulehe Formation deposits in the Qaidam Basin (Fig. 9A; Yin et al., 2008b). This distribution pattern of the Lulehe Formation deposits indicates that the Qaidam Basin was initiated as a common foreland basin during its earliest stage of sedimentation (Yin et al., 2002).

Sedimentology, facies analysis, and seismic reflection profiling provide evidence that the Lulehe Formation strata in the northern Qaidam Basin were deposited in a proximal foreland basin system. Therefore, we conclude that the Lulehe Formation deposits in the locality of Dahonggou originated from the proximal northern Qaidam Basin margin and the southern Qilian Shan.

Paleocurrent Evidence

The paleocurrent orientations of the deposits of the Lulehe Formation at Dahonggou are disputed (Fig. 1A). Three previous paleocurrent measurements of the continuous Cenozoic sequence at Dahonggou have been conducted (Fig. 10): Bush et al. (2016) and Ji et al. (2017) inferred dominantly SW- and SE-directed flows, transverse to and away from the southern Qilian Shan, throughout the Cenozoic. Wang et al. (2017) also inferred four SW-directed paleocurrent orientations within the lower Youshashan, upper Youshashan, and Shizigou Formation; however, they inferred two NE-directed paleocurrent directions within the Lulehe Formation and the lower part of the lower Ganchaigou Formation. Therefore, the sediment-dispersal pathways may have reversed during the interval between the lower Youshashan and lower Ganchaigou Formation.

To clarify the dispute over the provenance of the Lulehe Formation, we measured three paleocurrent orientations (PC-5, PC-6, PC-7) at three different horizons of the eastern Dahonggou section (Figs. 1B and 4). The results indicate SW- and SE-directed flows and a northerly source area. In addition, we obtained six paleocurrent estimates for the Lulehe Formation from the localities at Lulehe, Yuqia, and Yinmaxia in the northern Qaidam Basin (Figs. 1C–1E and 4). Except for two NE-directed flows for Lulehe, the other localities showed SW- to SE-directed flows (Fig. 4). We conclude that the two NE-directed flows at the Lulehe locality reflect the tectonic uplift of the adjacent Saishenteng Shan (Fig. 4).

In summary, all our paleocurrent analyses spanning a wide range of the northern Qaidam Basin confirm that the widespread Lulehe Formation deposits in the northern Qaidam Basin were derived from the northern Qaidam Basin margin and the southern Qilian Shan. These paleocurrent results are supported by other paleocurrent studies in the northern Qaidam Basin (Zhuang et al., 2011; Meng and Fang, 2008).

Evidence from Zircon U-Pb Ages

Comparisons of age distributions based on the presence and absence of specific ages or age groups are the most reliable means for provenance identification (Gehrels et al., 2011). Since numerous geological factors may bias zircon age distributions, including recycling of zircons from older sedimentary units exposed in source terranes and/or incorporation of detrital zircons during transport, variations in the proportions of ages or age groups should be used with caution (Gehrels et al., 2011).

Two previous studies have examined the detrital age structure of the Dahonggou sedimentary rocks, both based on seven sandstone samples (Bush et al., 2016; Wang et al., 2017). Compared to the sampling strategy of Wang et al. (2017), the samples of Bush et al. (2016) had a more uniform distribution. Both studies revealed two major age populations, Permian–Triassic (200–300 Ma) and late Cambrian to Early Devonian (500–400 Ma), and two minor age populations, Neoproterozoic (1000–700 Ma) and Paleoproterozoic (2.5–1.6 Ga). The depth of 3200–4300 m is an exception, and here the Permian–Triassic peak is minor or absent (Fig. 11). This age structure is inconsistent with the concept of a simplified two-stage evolution with a major 250 Ma peak being replaced by a major 440 Ma peak (Wang et al., 2017).

We combined large amounts of data to characterize several potential source terranes for the Cenozoic Dahonggou strata, including the East Kunlun Shan and Qimen Tagh (Fig. 6E; He et al., 2016; Li et al., 2013; Xia et al., 2015), Qilian Shan and Nan Shan (Fig. 6D; Chen et al., 2012; Gehrels et al., 2011, 2003a; Menold et al., 2009), and Mesozoic strata in the northern Qaidam Basin (Fig. 6B; Yu et al., 2017; Bush et al., 2016; this study). Compared to the age populations of the Cenozoic Dahonggou strata (Fig. 6C), those of the Qilian Shan and Nan Shan have fewer Permian–Triassic (300–200 Ma) ages, and those of the East Kunlun Shan and Qimen Tagh have fewer Paleoproterozoic (2.5–1.6 Ga) ages. Although their proportions vary considerably, the four age populations of the Cenozoic Dahonggou strata are all indicative of three potential source terranes. Therefore, it is difficult to tie zircons of these ages to specific source terranes, if we determine source terrane based on the presence or absence of specific age populations, rather than by variations in the proportions of the age populations.

Wang et al. (2017) suggested a two-stage provenance evolution model, with the earlier source area of the East Kunlun Shan being replaced by the Qilian Shan. This model is based mainly on the observation that granite bodies in the Qilian Shan are dominantly late Cambrian to early Devonian (500–400 Ma) in age, whereas those in the East Kunlun Shan are Permian–Triassic (300–200 Ma) in age. However, this assumption overlooks the fact that large amounts of zircons with crystallization ages of 300–200 Ma are present in the northern Qaidam Basin. Besides the occurrence of isolated plutons immediately north of the Dahonggou section in the northern Qaidam Basin (Chen et al., 2012; Cheng et al., 2017; Menold et al., 2009), the Jurassic and Cretaceous sedimentary rocks have a major zircon age peak of ca. 250 Ma (Bush et al., 2016; Yu et al., 2017; Qian et al., 2018).

Geological mapping and analyses of seismic reflection profiles indicate that the northern Qaidam Basin margin and the southern Qilian Shan–Nan Shan thrust belt developed a SW-directed thrust-wedge duplex (triangle-zone structure), the southward propagation of which has accommodated a significant amount of crustal shortening (20% to >60%; Yin et al., 2008a). The structural development of the orogenic wedge controls the geometry and shape of the northern Qaidam Basin and therefore has a strong influence on the prolonged exhumation of older strata within the fold-and-thrust belt and rapid sedimentation of younger strata within the basin interior. The Jurassic and Cretaceous sedimentary rocks crop out discontinuously within the fold-and-thrust belt of the northern Qaidam Basin margin with a greater altitude than the basin interior (Ritts and Biffi, 2001; Yu et al., 2017). It is believed that these Mesozoic rocks experienced multiphase exhumation and prolonged erosion since, or soon after, the beginning of the India-Eurasia collision (Yin et al., 2008a), and therefore they supplied large amounts of detritus to be redeposited within the basin interior. This interpretation was substantiated by recent detrital apatite fission-track analyses of Mesozoic strata in the northern Qaidam Basin margin, which suggested >6 km of exhumation of Mesozoic sedimentary rocks based on the observation that their apatite fission-track ages are

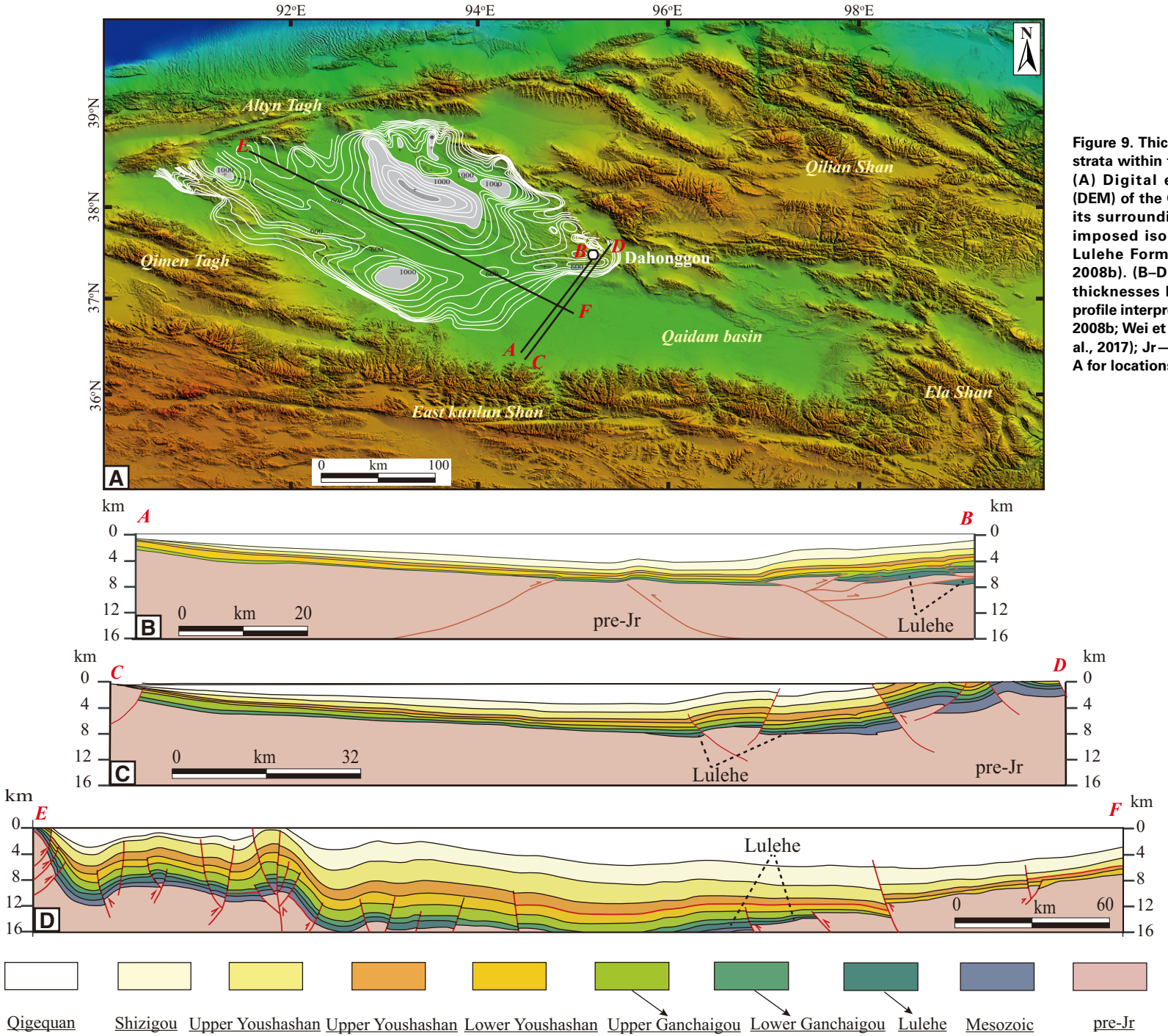

Figure 9. Thickness of Cenozoic strata within the Qaidam Basin. (A) Digital elevation model (DEM) of the Qaidam Basin and its surroundings, with superimposed isopach map of the Lulehe Formation (Yin et al., 2008b). (B–D) Cenozoic strata thicknesses based on seismic profile interpretations (Yin et al., 2008b; Wei et al., 2016; Cheng et al., 2017); Jr—Jurassic. See part A for locations.

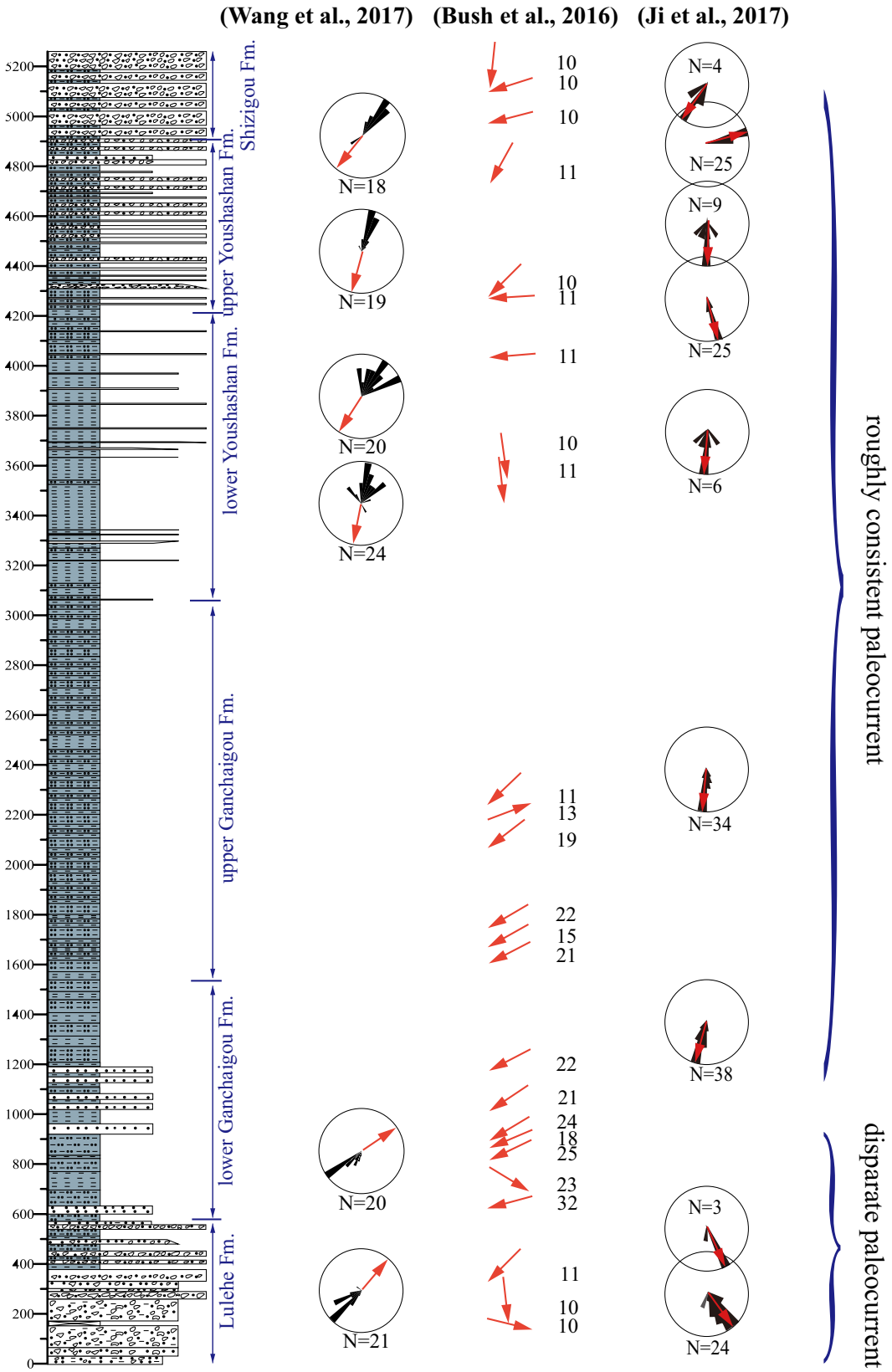

Figure 10. Measured 5.27-km-thick lithostratigraphic section of the western Dahonggou locality (Fig. 1B), with red arrows indicating mean paleocurrent vector within individual intervals. We deleted the paleocurrent data for the Cretaceous Quanyagou Formation from Bush et al. (2016). Studies have yielded roughly consistent paleocurrent data, except within the Lulehe and lower Ganchaigou Formations, where Bush et al. (2016) and Ji et al. (2017) inferred SE- or SW-directed paleocurrents, but Wang et al. (2017) inferred NE-directed paleocurrents. The lithological legend is the same as in Figure 8H.

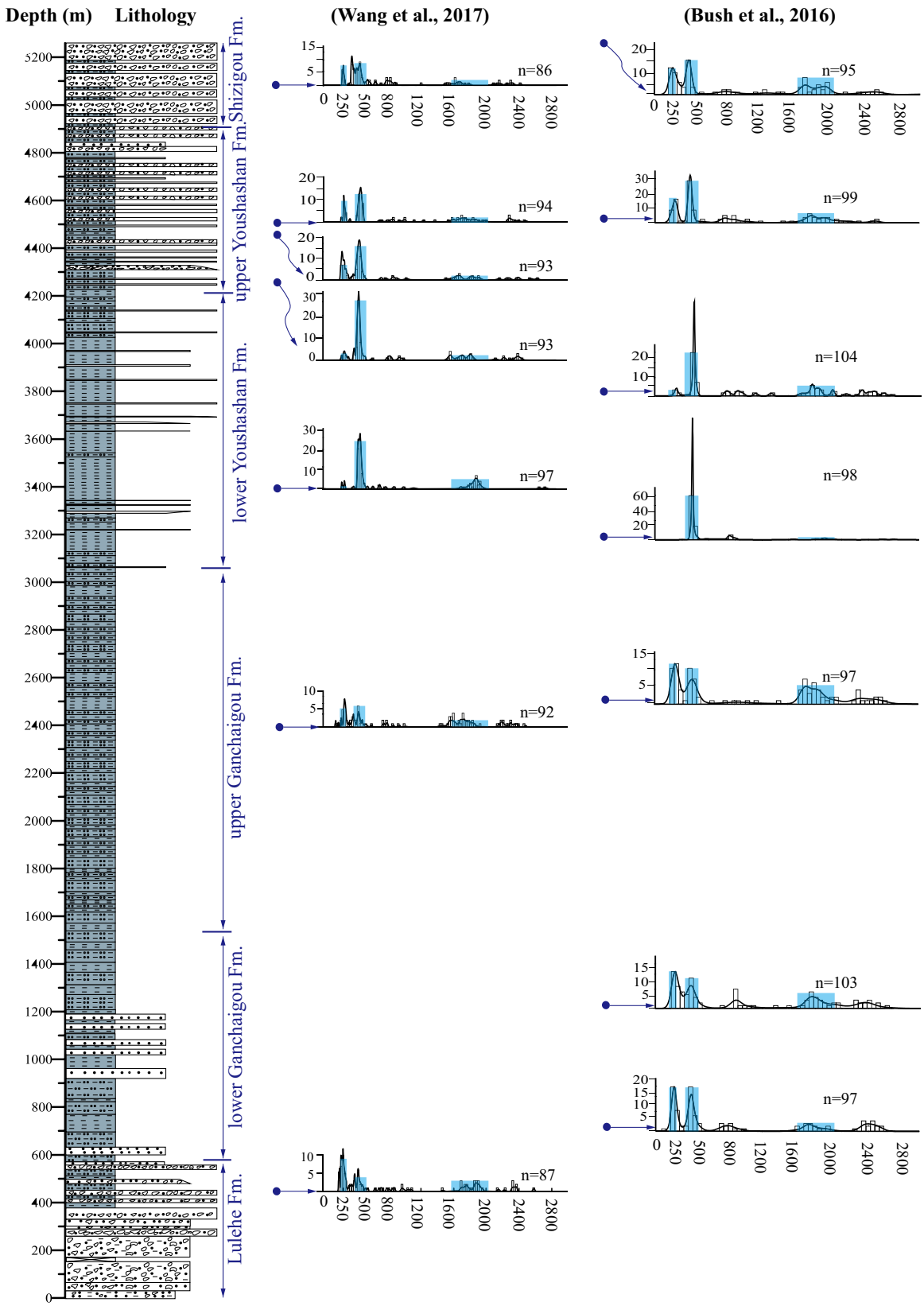

Figure 11. Results of two previous provenance studies based on U-Pb ages of detrital zircons, both based on seven samples from the Dahonggou section (Bush et al., 2016; Wang et al., 2017). We deleted the detrital zircon U-Pb geochronologic data for the Cretaceous Quanyagou Formation from Bush et al. (2016). The lithological legend is the same as in Figure 8H.

younger than their depositional ages (Jian et al., 2018). This sedimentary recycling model is further supported by sandstone compositional data. Numerous Cenozoic sandstone samples from the northern Qaidam Basin represent recycled orogenic or, more specifically, fold-and-thrust belt materials according to classical Dickinson-Gazzi variation diagrams (Fig. 12; Lu et al., 2014; Bush et al., 2016; Jian et al., 2013). Therefore, the Jurassic and Cretaceous sedimentary rocks in the northern Qaidam Basin margin could be one of the major source regions for the Cenozoic Dahonggou section, and recycling of these Mesozoic sedimentary units would yield Permian–Triassic–aged zircons, such as the 300–200 Ma population observed in the Cenozoic sandstones. Rieser et al. (2006b) reported a uniform 280–220 Ma age cluster for detrital white mica in Cenozoic sedimentary rocks from the Lulehe section in the northern Qaidam Basin (Fig. 1C). It was also concluded that these late Paleozoic–Early Triassic ages were either derived from recycled Triassic–Jurassic cover sequences, or from Permian intrusive bodies in the northern Qaidam Basin and the southern Qilian Shan–Nan Shan (Rieser et al., 2006b).

The widespread occurrence of 300–200 Ma detrital zircon ages in Mesozoic strata can be attributed to the fact that the bedrock of the Qaidam Basin contains granite bodies of 290–280 Ma to 215 Ma in age (Wu et al., 2016; Cheng et al., 2017; see Fig. 2C), which are overlain by Mesozoic–Cenozoic sedimentary rocks (Cheng et al., 2017). The episodic rejuvenation of fold-and-thrust belts (Ritts and Biffi, 2001), or normal faults (Yin et al., 2008a; Wu et al., 2011), in the northern Qaidam Basin since the Mesozoic may have exposed subsurface granites, which represent the principal and ultimate source for the 300–200 Ma detrital zircons in the Mesozoic and Cenozoic strata.

DISCUSSION

We obtained 500 detrital zircon ages from five Mesozoic sedimentary rocks, which were combined to supplement detrital zircon age data for Mesozoic strata in the northern Qaidam Basin. The integrated detrital zircon ages of Mesozoic strata show three major age populations: Permian–Triassic (300–200 Ma), late Cambrian to Early Devonian (500–400 Ma), and Paleoproterozoic (2.5–1.6 Ga), and one minor age population: Neoproterozoic (1000–700 Ma). Based on previous studies, the detrital zircon ages of the Cenozoic Dahonggou strata display two major age populations: Permian–Triassic (300–200 Ma) and late Cambrian to Early Devonian (500–400 Ma), and two minor age populations: Neoproterozoic (1000–700 Ma) and Paleoproterozoic (2.5–1.6 Ga). However, the four age populations are all reported in three potential source terranes, in varying proportions, including the East Kunlun Shan and Qimen Tagh, the Qilian Shan and Nan Shan, and Mesozoic strata in the northern Qaidam Basin. Therefore, it is difficult to tie zircons of these ages to specific source terranes using the presence or absence of specific age populations, rather than examining variations in the proportions of the age populations. Therefore, the use of a single detrital zircon dating method cannot provide unique source information.

Sedimentological analyses indicate that the Lulehe Formation strata at the Dahonggou locality are dominated by conglomeratic and sandy brick-red beds and were deposited first in an alluvial fan and then in a braided-fluvial system (Fig. 8). The Lulehe Formation deposits represent a high-gradient depositional system and synorogenic sedimentation, suggestive of a proximal uplifted source terrane (e.g., the northern Qaidam Basin margin and the southern Qilian Shan). Seismic reflection profiling also testifies that the Lulehe Formation strata in the northern Qaidam Basin were deposited in a proximal foreland basin system (Fig. 13). Therefore, sedimentological and stratigraphic evidence together indicate that the Lulehe Formation deposits at the Dahonggou locality originated from the proximal northern Qaidam Basin margin and the southern Qilian Shan (Fig. 13). This is further supported by our detailed paleocurrent studies spanning a large part of the northern Qaidam Basin (525 measurements at nine stations), which consistently indicate that the widespread Lulehe Formation deposits in the northern Qaidam Basin were derived from the northern Qaidam Basin margin and the southern Qilian Shan (Fig. 13).

Detrital fission-track dating can also be used to characterize variations in source terrane and has been regarded as a very important supplementary means of investigating changes in provenance for the Qaidam Basin (Du et al., 2018; Jian et al., 2018; Wang et al., 2017; Y. Wang et al., 2015). Detrital apatite fission-track data of the Cenozoic strata, especially the Lulehe Formation in the northern Qaidam Basin, show a prominent age population peak of 80–40 Ma (Du et al., 2018; Wang et al., 2017; Jian et al., 2018). This means that some of the Lulehe Formation sediments in the northern Qaidam Basin were most likely derived from Mesozoic strata in the northern Qaidam Basin margin, the detrital apatite fission-track ages of which range from 81 to 46 Ma (Fig. 13; Jian et al., 2018). Reworking of Mesozoic strata in response to uplift and cannibalization in the fold-and-thrust belt is supported by the presence of significant sedimentary lithic (Ls) grains and detrital modal analyses of Cenozoic sandstones in the northern Qaidam Basin, as was discussed above. It is thought that these Mesozoic strata experienced deep burial (>6 km) and strong annealing, resulting in younger detrital apatite fission-track ages than their depositional ages (Jian

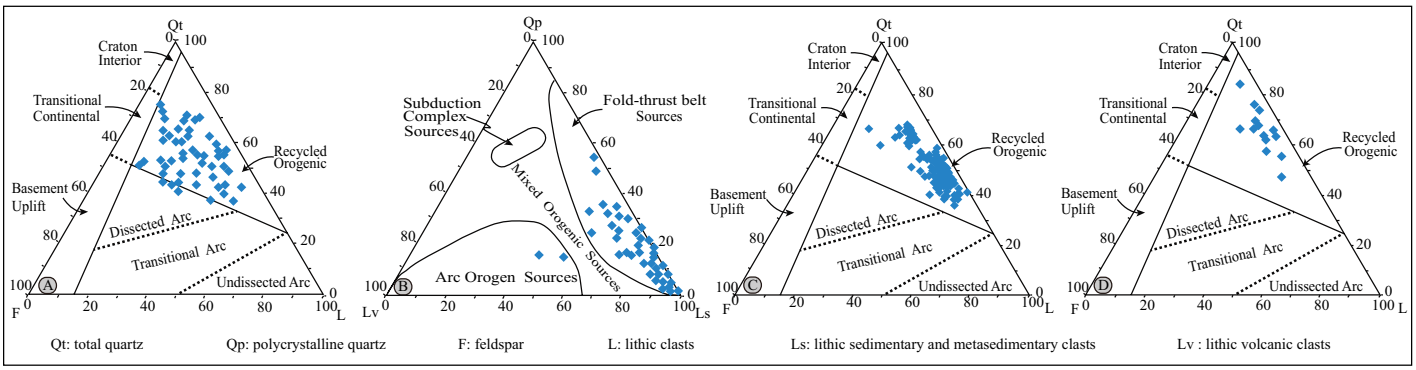

Figure 12. Quartz–feldspar–total lithic fragments (Qt-F-L) and polycrystalline quartz-lithic sedimentary clasts-lithic volcanic clasts (Qp-Lv-Ls) ternary diagrams of framework grain compositions of Cenozoic sandstones in the northern Qaidam Basin. (A–B) 150 sandstone samples from the northern Qaidam Basin spanning the Lulehe to Shizigou Formations, modified from Jian et al. (2013). (C) 129 sandstone samples collected from the upper Ganchaigou, lower Youshashan, and upper Youshashan Formations at the Dahonggou section (Lu et al., 2014). (D) 14 sandstone samples from the Dahonggou section, modified from Bush et al. (2016). Fields of various tectonic settings are from Dickinson (1985).

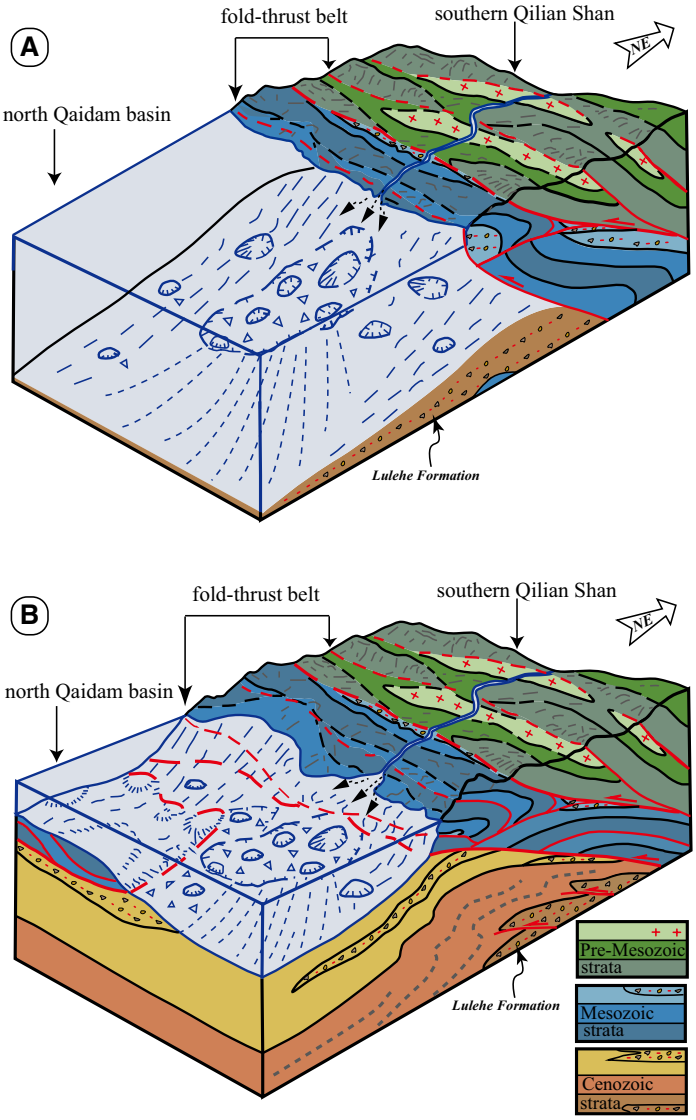

Figure 13. Schematic block diagrams illustrating the source-sink relationships between the southern Qilian Shan and Mesozoic–Cenozoic strata in the northern Qaidam Basin, adapted from Plašienka (2012). (A) Tectono-sedimentary framework during the sedimentation of the Lulehe Formation. At this time, the bedrocks of the southern Qilian Shan and Mesozoic strata in the northern Qaidam Basin were the predominant sources of Cenozoic strata in the northern Qaidam Basin. This framework highlights the significance of the recycled orogen effect of Mesozoic strata in the fold-and-thrust belt of the northern Qaidam Basin. (B) Present tectono-sedimentary framework of the northern Qaidam Basin. In this diagram, the Cenozoic strata are a major source area of the Quaternary sediments.

et al., 2018). Wang et al. (2017) suggested a drastic change of source area, with an early southerly source area (East Kunlun Shan) being replaced by a subsequent northerly source area (the southern Qilian Shan), based on the observations that an early sharp decrease in peak ages up section was succeeded by a slowly decreasing trend of peak ages. However, this conclusion is unconvincing, since it is based solely on sharp variations in detrital apatite fission-track ages. Jian et al. (2018) also observed similar variations in detrital thermochronological data, but they attributed the phenomenon to a single massive source area (the northern Qaidam Basin margin and the southern Qilian Shan) with distinct cooling ages. Low-temperature thermochronological studies of crystalline basement rocks suggest that the northern Qaidam Basin margin (Lvliang Shan and Xitie Shan) and the southern Qilian Shan had a regionally heterogeneous cooling history, which indicates three phases of rapid exhumation since the Mesozoic (Early Cretaceous, Paleocene–Eocene and middle–late Miocene; X. Cheng et al., 2016; Jolivet et al., 2001; Wang et al., 2004; Zhuang et al., 2018).

This provenance model has important implications for the timing of the tectonic uplift of the northern Qaidam Basin margin and the southern Qilian Shan. The age of the basal Cenozoic sedimentary rocks in the Qaidam Basin (the basal age of the Lulehe Formation) is bracketed to 65–50 Ma (Ji et al., 2017; Yin et al., 2008a), or ca. 25 Ma (Wang et al., 2017). Since these massive terrigenous clastic sedimentary rocks in the northern Qaidam Basin are the product of surface uplift, tectonic exhumation, and erosion of the northern Qaidam Basin margin and the southern Qilian Shan, the timing of the initiation of surface uplift of the northern Qaidam Basin margin and the southern Qilian Shan was likely no later than 65–50 Ma, or ca. 25 Ma. Irrespective of which age is correct, the substantial uplift of the southern Qilian Shan should be far older than 12 Ma, as suggested by Wang et al. (2017).

CONCLUSIONS

Our integrated study of the sedimentology, paleocurrent directions, detrital zircon U-Pb ages, detrital apatite fission-track ages, and seismic reflection profiles enables us to assemble a reliable reconstruction of the provenance of the Lulehe Formation in the northern Qaidam Basin.

(1) The detrital zircon age populations of the Cenozoic Dahonggou strata are all reported in three potential source terranes, in varying proportions, including the East Kunlun Shan and Qimen Tagh, the Qilian Shan and Nan Shan, and Mesozoic strata in the northern Qaidam Basin. Thus, the use of a single detrital zircon dating method cannot provide unique source information.

(2) The sedimentological and paleocurrent analyses, in combination with existing paleocurrent data, seismic reflection data, and detrital apatite fission-track dating, point consistently to a unified proximal northerly source area (the northern Qaidam Basin margin and the southern Qilian Shan).

(3) The orogenic recycling effect of Mesozoic strata in the fold-and-thrust belt of the northern Qaidam Basin, which was ignored in recent studies, played a significant role in producing the Permian–Triassic–aged zircons observed in the Cenozoic sandstones.

ACKNOWLEDGMENTS

We thank Longgang Fan, Guoli Wu, and Xuxuan Ma for help with data processing and interpretations; Aijun Sun for help in the field; and Min Lei and Xiangzhen Xu for providing laboratory support. Laurent Godin (Science Editor) and two anonymous reviewers are thanked for constructive and valuable suggestions. This research was supported by the National Natural Science Foundation of China (grant 41472187), the Strategic Priority Research Program of the Chinese Academy of Sciences (grant XDA19050104), and the China Geological Survey (grant DD20160022–03).

REFERENCES CITED

Bush, M., Saylor, J., Horton, B., and Nie, J., 2016, Growth of the Qaidam Basin during Cenozoic exhumation in the northern Tibetan Plateau: Inferences from depositional patterns and multiproxy detrital provenance signatures: Lithosphere, v. 8, p. 58–82, https://doi.org/10.1130/L449.1.

Carter, A., and Moss, S.J., 1999, Combined detrital-zircon fission-track and U-Pb dating: A new approach to understanding hinterland evolution: Geology, v. 27, no. 3, p. 235–238, https://doi.org/10.1130/0091-7613(1999)027<0235:CDZFTA>2.3.CO;2.

Chang, H., Li, L., Qiang, X., Garzione, C.N., Pullen, A., and An, Z., 2015, Magnetostratigraphy of Cenozoic deposits in the western Qaidam Basin and its implication for the surface uplift of the northeastern margin of the Tibetan Plateau: Earth and Planetary Science Letters, v. 430, p. 271–283, https://doi.org/10.1016/j.epsl.2015.08.029.

Chen, X., Gehrels, G., Yin, A., Li, L., and Jiang, R., 2012, Paleozoic and Mesozoic basement magmatisms of eastern Qaidam Basin, northern Qinghai-Tibet Plateau: LA-ICP-MS zircon U-Pb geochronology and its geological significance: Acta Geologica Sinica [English Edition], v. 86, no. 2, p. 350–369, https://doi.org/10.1111/j.1755-6724.2012.00665.x.

Chen, X., Yin, A., Gehrels, G.E., Cowgill, E.S., Grove, M., Harrison, T.M., and Wang, X.F., 2003, Two phases of Mesozoic north-south extension in the eastern Altyn Tagh range, northern Tibetan Plateau: Tectonics, v. 22, no. 5, TC1053, https://doi.org/10.1029/2001TC001336.

Cheng, F., Fu, S., Jolivet, M., Zhang, C., and Guo, Z., 2016a, Source to sink relation between the Eastern Kunlun Range and the Qaidam Basin, northern Tibetan Plateau, during the Cenozoic: Geological Society of America Bulletin, v. 128, no. 1, p. 258–283, https://doi.org/10.1130/B31260.1.

Cheng, F., Jolivet, M., Fu, S., Zhang, C., Zhang, Q., and Guo, Z., 2016b, Large-scale displacement along the Altyn Tagh fault (North Tibet) since its Eocene initiation: Insight from detrital zircon U-Pb geochronology and subsurface data: Tectonophysics, v. 677–678, p. 261–279, https://doi.org/10.1016/j.tecto.2016.04.023.

Cheng, F., Jolivet, M., Hallot, E., Zhang, D., Zhang, C., and Guo, Z., 2017, Tectono-magmatic rejuvenation of the Qaidam craton, northern Tibet: Gondwana Research, v. 49, p. 248–263, https://doi.org/10.1016/j.gr.2017.06.004.

Cheng, X., Lin, X., Wu, L., Chen, H., Xiao, A., Gong, J., Zhang, F., and Yang, S., 2016, The Exhumation history of North Qaidam thrust belt constrained by apatite fission track thermochronology: Implication for the rvolution of the Tibetan Plateau: Acta Geologica Sinica [English Edition], v. 90, no. 3, p. 870–883, https://doi.org/10.1111/1755-6724.12730.

Cowgill, E., Yin, A., Harrison, T.M., and Wang, X., 2003, Reconstruction of the Altyn Tagh fault based on U-Pb geochronology: Role of back thrusts, mantle sutures, and heterogeneous crustal strength in forming the Tibetan Plateau: Journal of Geophysical Research–Solid Earth, v. 108, no. B7, p. 457–470.

DeCelles, P.G., Gray, M.B., Ridgway, K.D., Cole, R.B., Pivnik, D.A., Pequera, N., and Srivastava, P., 1991, Controls on synorogenic alluvial-fan architecture, Beartooth Conglomerate (Palaeocene), Wyoming and Montana: Sedimentology, v. 38, no. 4, p. 567–590, https://doi.org/10.1111/j.1365-3091.1991.tb01009.x.

DeCelles, P.G., Kapp, P., Gehrels, G.E., and Ding, L., 2014, Paleocene–Eocene foreland basin evolution in the Himalaya of southern Tibet and Nepal: Implications for the age of initial India-Asia collision: Tectonics, v. 33, no. 5, p. 824–849, https://doi.org/10.1002/2014TC003522.

Dickinson, W. R., 1985, Interpreting provenance relations from detrital modes of sandstones, *in* Zuffa, G.G., ed., Provenance of Arenites: New York, D. Reidel Publishing, North Atlantic Treaty Organization (NATO) Advanced Study Institute (ASI) Series C: Mathematical and Physical Sciences Volume 148, p. 333–361.

Du, D., Zhang, C., Mughal, M. S., Wang, X., Blaise, D., Gao, J., Ma, Y., and Luo, X., 2018, Detrital apatite fission track constraints on Cenozoic tectonic evolution of the north eastern Qinghai-Tibet Plateau, China: Evidence from Cenozoic strata in Lulehe section, the northern Qaidam Basin: Journal of Mountain Science, v. 15, no. 3, p. 532–547, https://doi.org/10.1007/s11629-017-4692-5.

Fang, X., Zhang, W., Meng, Q., Gao, J., Wang, X., King, J., Song, C., Dai, S., and Miao, Y., 2007, High-resolution magnetostratigraphy of the Neogene Huaitoutala section in the eastern Qaidam Basin on the NE Tibetan Plateau, Qinghai Province, China, and its implication on tectonic uplift of the NE Tibetan Plateau: Earth and Planetary Science Letters, v. 258, no. 1, p. 293–306, https://doi.org/10.1016/j.epsl.2007.03.042.

Fu, L., Guan, P., Zhao, W., Wang, M., Zhang, Y., and Lu, J., 2013, Heavy mineral feature and provenance analysis of Paleogene Lulehe Formation in Qaidam Basin: Acta Petrologica Sinica, v. 29, no. 8, p. 2867–2875 [in Chinese with English abstract].

Fu, S., Ma, D., Guo, Z., and Cheng, F., 2015, Strike-slip superimposed Qaidam Basin and its control on oil and gas accumulation, NW China: Petroleum Exploration and Development, v. 42, no. 6, p. 778–789, https://doi.org/10.1016/S1876-3804(15)30074-4.

Garzanti, E., Baud, A., and Mascle, G., 1987, Sedimentary record of the northward flight of India and its collision with Eurasia (Ladakh Himalaya, India): Geodinamica Acta, v. 1, p. 297–312, https://doi.org/10.1080/09853111.1987.11105147.

Garzanti, E., Critelli, S., and Ingersoll, R.V., 1996, Paleogeographic and paleotectonic evolution of the Himalayan Range as reflected by detrital modes of Tertiary sandstones and modern sands (Indus transect, India and Pakistan): Geological Society of America Bulletin, v. 108, p. 631–642, https://doi.org/10.1130/0016-7606(1996)108<0631:PAPEOT>2.3.CO;2.

Gehrels, G.E., Yin, A., and Wang, X., 2003a, Detrital-zircon geochronology of the northeastern Tibetan Plateau: Geological Society of America Bulletin, v. 115, no. 7, p. 881–896, https://doi.org/10.1130/0016-7606(2003)115<0881:DGOTNT>2.0.CO;2.

Gehrels, G.E., Yin, A., and Wang, X., 2003b, Magmatic history of the northeastern Tibetan Plateau: Journal of Geophysical Research–Solid Earth, v. 108, no. B9, 2423, https://doi.org/10.1029/2002JB001876.

Gehrels, G., Kapp, P., DeCelles, P., Pullen, A., Blakey, R., Weislogel, A., Ding, L., Guynn, J., Martin, A., McQuarrie, N., and Yin, A., 2011, Detrital zircon geochronology of pre-Tertiary strata in the Tibetan-Himalayan orogen: Tectonics, v. 30, no. 5, TC5016, https://doi.org/10.1029/2011TC002868.

Hanson, A.D., 1999, Organic Geochemistry and Petroleum Geology, Tectonics and Basin Analysis of the Southern Tarim and Northern Qaidam Basins, Northwest China [Ph.D. dissertation]: Stanford, California, Stanford University, 388 p.

He, D., Dong, Y., Liu, X., Yang, Z., Sun, S., Cheng, B., and Li, W., 2016, Tectono-thermal events in East Kunlun, northern Tibetan Plateau: Evidence from zircon U-Pb geochronology: Gondwana Research, v. 30, p. 179–190, https://doi.org/10.1016/j.gr.2015.08.002.

Heermance, R.V., Pullen, A., Kapp, P., Garzione, C.N., Bogue, S., Ding, L., and Song, P., 2013, Climatic and tectonic controls on sedimentation and erosion during the Pliocene–Quaternary in the Qaidam Basin (China): Geological Society of America Bulletin, v. 125, no. 5–6, p. 833–856, https://doi.org/10.1130/B30748.1.

Horton, B.K., Yin, A., Spurlin, M.S., Zhou, J., and Wang, J., 2002, Paleocene–Eocene syncontractional sedimentation in narrow, lacustrine-dominated basins of east-central Tibet: Geological Society of America Bulletin, v. 114, p. 771–786, https://doi.org/10.1130/0016-7606(2002)114<0771:PESSIN>2.0.CO;2.

Huang, H., Huang, Q., and Ma, Y., 1996, Geology of Qaidam Basin and its Petroleum Prediction: Beijing, Geological Publishing House, 257 p.

Ji, J., Zhang, K., Clift, P., Zhuang, G., Song, B., Ke, X., and Xu, Y., 2017, High-resolution magnetostratigraphic study of the Paleogene–Neogene strata in the northern Qaidam Basin: Implications for the growth of the northeastern Tibetan Plateau: Gondwana Research, v. 46, p. 141–155, https://doi.org/10.1016/j.gr.2017.02.015.

Jian, X., Guan, P., Zhang, D., Zhang, W., Feng, F., Liu, R., and Lin, S., 2013, Provenance of Tertiary sandstone in the northern Qaidam Basin, northeastern Tibetan Plateau: Integration of framework petrography, heavy mineral analysis and mineral chemistry: Sedimentary Geology, v. 290, p. 109–125, https://doi.org/10.1016/j.sedgeo.2013.03.010.

Jian, X., Guan, P., Zhang, W., Liang, H., Feng, F., and Fu, L., 2018, Late Cretaceous to early Eocene deformation in the northern Tibetan Plateau: Detrital apatite fission track evidence from the northern Qaidam Basin: Gondwana Research, v. 60, p. 94–104, https://doi.org/10.1016/j.gr.2018.04.007.

Jolivet, M., Brunel, M., Seward, D., Xu, Z., Yang, J., Roger, F., Tapponnier, P., Malavieille, J., Arnaud, N., and Wu, C., 2001, Mesozoic and Cenozoic tectonics of the northern edge of the Tibetan Plateau: Fission-track constraints: Tectonophysics, v. 343, p. 111–134, https://doi.org/10.1016/S0040-1951(01)00196-2.

Kapp, P., Decelles, P.G., Gehrels, G.E., Heizler, M., and Ding, L., 2007, Geological records of the Cretaceous Lhasa-Qiangtang and Indo-Asian collisions in the Nima Basin area, central Tibet: Geological Society of America Bulletin, v. 119, p. 917–933, https://doi.org/10.1130/B26033.1.

Li, L., Garzione, C.N., Pullen, A., Zhang, P., Li, Y., Li, L., Garzione, C.N., Pullen, A., Zhang, P., and Li, Y., 2017, Late Cretaceous–Cenozoic basin evolution and topographic growth of the Hoh Xil Basin, central Tibetan Plateau: Geological Society of America Bulletin, v. 130, no. 3, p. 499–521.

Li, W., Neubauer, F., Liu, Y., Genser, J., Ren, S., Han, G., and Liang, C., 2013, Paleozoic evolution of the Qimantagh magmatic arcs, Eastern Kunlun Mountains: Constraints from zircon dating of granitoids and modern river sands: Journal of Asian Earth Sciences, v. 77, p. 183–202, https://doi.org/10.1016/j.jseaes.2013.08.030.

Liu, Z., 1988, Geologic Map of the Qinghai-Xizang Plateau and its Neighboring Regions: Beijing, Geologic Publishing House, and Chengdu Institute of Geology and Mineral Resources, scale 1:1,500,000.

Lu, H., and Xiong, S., 2009, Magnetostratigraphy of the Dahonggou section, the northern Qaidam Basin, and its bearing on Cenozoic tectonic evolution of the Qilian Shan and Altyn Tagh fault: Earth and Planetary Science Letters, v. 288, no. 3–4, p. 539–550, https://doi.org/10.1016/j.epsl.2009.10.016.

Lu, H., Wang, E., and Meng, K., 2014, The mid-Miocene tectonic uplift of the southern Qilianshan: Sedimentary evidence from Dahonggou section in Qaidam Basin: Chinese Journal of Geology, v. 45, no. 1, p. 95–103.

Mao, L., Xiao, A., Zhang, H., Wu, Z., Wang, L., Shen, Y., and Wu, L., 2016, Structural deformation pattern within the NW Qaidam Basin in the Cenozoic era and its tectonic implications: Tectonophysics, v. 687, p. 78–93, https://doi.org/10.1016/j.tecto.2016.09.008.

McBride, E.F., 1963, A classification of common sandstones: Journal of Sedimentary Research, v. 33, p. 664–669.

Meng, Q., and Fang, X., 2008, Cenozoic tectonic development of the Qaidam Basin in the northeastern Tibetan Plateau, *in* Burchfiel, B.C., and Wang, E., eds., Investigations into the Tectonics of the Tibetan Plateau: Geological Society of America Special Paper 444, p. 1–24, https://doi.org/10.1130/2008.2444(01).

Meng, Q., Hu, J., and Yang, F., 2001, Timing and magnitude of displacement on the Altyn Tagh fault: Constraints from stratigraphic correlation of adjoining Tarim and Qaidam Basins, NW China: Terra Nova, v. 13, no. 2, p. 86–91, https://doi.org/10.1046/j.1365-3121.2001.00320.x.

Menold, C.A., Manning, C.E., Yin, A., Tropper, P., Chen, X.H., and Wang, X.F., 2009, Metamorphic evolution, mineral chemistry and thermobarometry of orthogneiss hosting ultrahigh-pressure eclogites in the North Qaidam metamorphic belt, western China: Journal of Asian Earth Sciences, v. 35, no. 3–4, p. 273–284, https://doi.org/10.1016/j.jseaes.2008.12.008.

Metivier, F., Gaudemer, Y., Tapponnier, P., and Meyer, B., 1998, Northeastward growth of the Tibet plateau deduced from balanced reconstruction of two depositional areas: The Qaidam and Hexi Corridor basins, China: Tectonics, v. 17, no. 6, p. 823–842, https://doi.org/10.1029/98TC02764.

Miall, A.D., 1978, Lithofacies types and vertical profile models in braided river deposits: A summary, *in* Miall, A.D., ed., Fluvial Sedimentology: Canadian Society of Petroleum Geologists Memoir 5, p. 597–604.

Najman, Y., 2006, The detrital record of orogenesis: A review of approaches and techniques used in the Himalayan sedimentary basins: Earth-Science Reviews, v. 74, p. 1–72.

Pan, G., Ding, J., Yao, D., and Wang, L., 2004, Geological map of Qinghai-Xiang (Tibet) Plateau and Adjacent Areas: Chengdu, China, Chengdu Cartographic Publishing House, and Chengdu Institute of Geology and Mineral Resources, China Geological Survey, scale 1:1,500,000.

Plašienka, D., 2012, Jurassic syn-rift and Cretaceous syn-orogenic, coarse-grained deposits related to opening and closure of the Vahic (South Penninic) Ocean in the Western Carpathians–an overview: Geological Quarterly, v. 56, p. 601–628, https://doi.org/10.7306/gq.1044.

Qinghai Bureau of Geology and Mineral Resources (QBGMR), 1980, Geologic Map of the Mahai Sheet: Beijing, Geological Publishing House, scale 1:200,000.

Qinghai Bureau of Geology and Mineral Resources (QBGMR), 1984, Geologic Map of the Daqaidam Sheet: Beijing, Geological Publishing House, scale 1:200,000.

Qian, T., Wang, Z., Liu, Y., Liu, S., Gao, W., Li, W., Hu, J., and Li, L., 2018, Provenance analysis of the Jurassic the northern Qaidam Basin: Stratigraphic succession and LA-ICP-MS geochronology: Scientia Sinica Terrae, v. 48, p. 224–242 [in Chinese with English abstract].

Rieser, A.B., Neubauer, F., Liu, Y., and Ge, X., 2005, Sandstone provenance of north-western sectors of the intracontinental Cenozoic Qaidam Basin, western China: Tectonic vs. climatic control: Sedimentary Geology, v. 177, no. 1, p. 1–18, https://doi.org/10.1016/j.sedgeo.2005.01.012.

Rieser, A.B., Liu, Y., Genser, J., Neubauer, F., Handler, R., Friedl, G., and Ge, X.H., 2006a, $^{40}Ar/^{39}Ar$ ages of detrital white mica constrain the Cenozoic development of the intracontinental Qaidam Basin, China: Geological Society of America Bulletin, v. 118, no. 11, p. 65–68.

Rieser, A.B., Liu, Y., Genser, J., Neubauer, F., Handler, R., and Ge, X.H., 2006b, Uniform Permian $^{40}Ar/^{39}Ar$ detrital mica ages in the eastern Qaidam Basin (NW China): Where is the source?: Terra Nova, v. 18, no. 1, p. 79–87, https://doi.org/10.1111/j.1365-3121.2005.00666.x.

Ritts, B.D., and Biffi, U., 2001, Mesozoic northeast Qaidam Basin: Response to contractional reactivation of the Qilian Shan, and implications for the extent of Mesozoic intracontinental deformation in Central Asia, *in* Hendrix, M.S., and Davis, G.A., eds., Paleozoic and Mesozoic Tectonic Evolution of Central and Eastern Asia: From Continental Assembly to Intracontinental Deformation: Geological Society of America Memoir 194, p. 293–316, https://doi.org/10.1130/0-8137-1194-0.293.

Ritts, B.D., Yue, Y., and Graham, S.A., 2004, Oligocene–Miocene tectonics and sedimentation along the Altyn Tagh fault, northern Tibetan Plateau: Analysis of the Xorkol, Subei, and Aksay Basins: The Journal of Geology, v. 112, no. 2, p. 207–229, https://doi.org/10.1086/381658.

Ritts, B.D., Yue, Y., Graham, S.A., Sobel, E.R., Abbink, O.A., and Stockli, D., 2008, From sea level to high elevation in 15 million years: Uplift history of the northern Tibetan Plateau margin in the Altun Shan: American Journal of Science, v. 308, no. 5, p. 657–678, https://doi.org/10.2475/05.2008.01.

Song, B., Zhang, K., Lu, J., Wang, C., and Xu, Y., 2013, The middle Eocene to early Miocene integrated sedimentary record in the Qaidam Basin and its implications for paleoclimate and early Tibetan Plateau uplift: Canadian Journal of Earth Sciences, v. 50, p. 183–196, https://doi.org/10.1139/cjes-2012-0048.

Spurlin, M.S., Yin, A., Horton, B.K., Zhou, J., and Wang, J., 2005, Structural evolution of the Yushu-Nangqian region and its relationship to syncollisional igneous activity, east-central Tibet: Geological Society of America Bulletin, v. 117, no. 9–10, p. 1293–1317, https://doi.org/10.1130/B25572.1.

Staisch, L.M., Niemi, N.A., Chang, H., Clark, M.K., Rowley, D.B., and Brian, C., 2014, A Cretaceous–Eocene depositional age for the Fenghuoshan Group, Hoh Xil Basin: Implications for the tectonic evolution of the northern Tibet Plateau: Tectonics, v. 33, no. 3, p. 281–301, https://doi.org/10.1002/2013TC003367.

Sun, Z., Yang, Z., Pei, J., Ge, X., Wang, X., Yang, T., Li, W., and Yuan, S., 2005, Magnetostratigraphy of Paleogene sediments from the northern Qaidam Basin, China: Implications for tectonic uplift and block rotation in northern Tibetan Plateau: Earth and Planetary Science Letters, v. 237, no. 3, p. 635–646, https://doi.org/10.1016/j.epsl.2005.07.007.

Tapponnier, P., Xu, Z., Françoise, R., Bertrand, M., Nicolas, A., Gérard, W., and Yang, J., 2001, Oblique stepwise rise and growth of the Tibet plateau: Science, v. 294, no. 5547, p. 1671–1677, https://doi.org/10.1126/science.105978.

Turner, P., 1980, Continental Red Beds: New York, Elsevier Academic Press, Developments in Sedimentology 29, 562 p.

Wang, C., Li, R., Li, M., Meert, J.G., and Peng, Y., 2015, Palaeoproterozoic magmatic-metamorphic history of the Quanji Massif, Northwest China: Implications for a single North China–Quanji–Tarim craton within the Columbia supercontinent?: International Geology Review, v. 57, no. 13, p. 1772–1790, https://doi.org/10.1080/00206814.2015.1026849.

Wang, E., Xu, F.Y., Zhou, J.X., Wan, J., and Burchfiel, B.C., 2006, Eastward migration of the Qaidam Basin and its implications for Cenozoic evolution of the Altyn Tagh fault and associated river systems: Geological Society of America Bulletin, v. 118, no. 3–4, p. 349–365, https://doi.org/10.1130/B25778.1.

Wang, F., Lo, C., Li, Q., Yeh, M., Wan, J., Zheng, D., and Wang, E., 2004, Onset timing of significant unroofing around Qaidam Basin, northern Tibet, China: Constraints from $^{40}Ar/^{39}Ar$ and FT thermochronology on granitoids: Journal of Asian Earth Sciences, v. 24, p. 59–69, https://doi.org/10.1016/j.jseaes.2003.07.004.

Wang, J., Hu, X., Jansa, L., and Huang, Z., 2011, Provenance of the Upper Cretaceous–Eocene deep-water sandstones in Sangdanlin, southern Tibet: Constraints on the timing of initial India-Asia collision: The Journal of Geology, v. 119, no. 3, p. 293–309, https://doi.org/10.1086/659145.

Wang, L.Q., Pan, G.T., Ding, J., and Yao, D.S., 2013, Geological Map of the Tibetan Plateau (scale at 1:1,500,000) with Explanations: Beijing, Geological Publishing House, 288 p.

Wang, W., Zheng, W., Zhang, P., Li, Q., Kirby, E., Yuan, D., Zheng, D., Liu, C., Wang, Z., Zhang, H., and Pang, J., 2017, Expansion of the Tibetan Plateau during the Neogene: Nature Communications, v. 8, p. 15887, https://doi.org/10.1038/ncomms15887.

Wang, Y., Zheng, J., Zheng, Y., Liu, X., and Sun, G., 2015, Paleocene–early Eocene uplift of the Altyn Tagh Mountain: Evidence from detrital zircon fission track analysis and seismic sections in the northwestern Qaidam Basin: Journal of Geophysical Research–Solid Earth, v. 120, no. 12, p. 8534–8550, https://doi.org/10.1002/2015JB011922.

Wei, Y., Xiao, A., Wu, L., Mao, L., Zhao, H., Shen, Y., and Wang, L., 2016, Temporal and spatial patterns of Cenozoic deformation across the Qaidam Basin, northern Tibetan Plateau: Terra Nova, v. 28, no. 6, p. 409–418, https://doi.org/10.1111/ter.12234.

Wu, C., Yin, A., Zuza, A.V., Zhang, J., Liu, W., and Ding, L., 2016, Pre-Cenozoic geologic history of the central and northern Tibetan Plateau and the role of Wilson cycles in constructing the Tethyan orogenic system: Lithosphere, v. 8, no. 3, p. 254–292, https://doi.org/10.1130/L494.1.

Wu, F., Ji, W., Wang, J., Liu, C., Chung, S., and Clift, P.D., 2014, Zircon U-Pb and Hf isotopic constraints on the onset time of India-Asia collision: American Journal of Science, v. 314, no. 2, p. 548–579, https://doi.org/10.2475/02.2014.04.

Wu, L., Xiao, A., Wang, L., Shen, Z., Zhou, S., Chen, Y., Wang, L., Liu, D., and Guan, J., 2011, Late Jurassic–Early Cretaceous northern Qaidam Basin, NW China: Implications for the earliest Cretaceous intracontinental tectonism: Cretaceous Research, v. 32, no. 4, p. 552–564, https://doi.org/10.1016/j.cretres.2011.04.002.

Wu, L., Xiao, A., Yang, S., Wang, L., Mao, L., Wang, L., Dong, Y., and Xu, B., 2012, Two-stage evolution of the Altyn Tagh fault during the Cenozoic: New insight from provenance analysis of a geological section in NW Qaidam Basin, NW China: Terra Nova, v. 24, no. 5, p. 387–395, https://doi.org/10.1111/j.1365-3121.2012.01077.x.

Xinjiang Bureau of Geology and Mineral Resources (XBGMR), 1993, Regional Geology of Xinjiang Uygur Autonomous Region: Geological Memoir 1, Number 32 (scale 1:1,500,000): Beijing, Geological Publishing House, 843 p.

Xia, R., Wang, C., Qing, M., Deng, J., Carranza, E.J.M., Li, W., Guo, X., Ge, L., and Yu, W., 2015, Molybdenite Re-Os, zircon U-Pb dating and Hf isotopic analysis of the Shuangqing Fe-Pb-Zn-Cu skarn deposit, East Kunlun Mountains, Qinghai Province, China: Ore Geology Reviews, v. 66, p. 114–131, https://doi.org/10.1016/j.oregeorev.2014.10.024.

Xia, W., Zhang, N., Yuan, X., Fan, L., and Zhang, B., 2001, Cenozoic Qaidam Basin, China: A stronger tectonic inversed, extensional rifted basin: American Association of Petroleum Geologists Bulletin, v. 85, no. 4, p. 715–736.

Yang, J.S., 2002, Early Paleozoic North Qaidam UHP metamorphic belt on the northeastern Tibetan Plateau and a paired subduction model: Terra Nova, v. 14, p. 397–404, https://doi.org/10.1046/j.1365-3121.2002.00438.x.

Yin, A., 2010, Cenozoic tectonic evolution of Asia: A preliminary synthesis: Tectonophysics, v. 488, p. 293–325, https://doi.org/10.1016/j.tecto.2009.06.002.

Yin, A., and Harrison, T.M., 2000, Geologic evolution of the Himalayan-Tibetan orogen: Annual Review of Earth and Planetary Sciences, v. 28, p. 211–280, https://doi.org/10.1146/annurev.earth.28.1.211.

Yin, A., Rumelhart, P.E., Butler, R., Cowgill, E., Harrison, T., Foster, D., and Ingersoll, R., 2002, Tectonic history of the Altyn Tagh fault system in northern Tibet inferred from Cenozoic sedimentation: Geological Society of America Bulletin, v. 114, no. 10, p. 1257–1295, https://doi.org/10.1130/0016-7606(2002)114<1257:THOTAT>2.0.CO;2.

Yin, A., Dang, Y.Q., Zhang, M., McRivette, M.W., Burgess, W.P., and Chen, X.H., 2007a, Cenozoic tectonic evolution of Qaidam Basin and its surrounding regions (Part 2): Wedge tectonics in southern Qaidam Basin and the Eastern Kunlun Range, *in* Sears, J.W., Harms, T.A., and Evenchick, C.A., eds., Whence the Mountains? Inquiries into the Evolution of Orogenic Systems: A Volume in Honor of Raymond A. Price: Geological Society of America Special Paper 433, p. 369–390, https://doi.org/10.1130 /2007.2433 (18).

Yin, A., Manning, C.E., Lovera, O., Menold, C.A., Chen, X., and Gehrels, G.E., 2007b, Early Paleozoic tectonic and thermomechanical evolution of ultrahigh-pressure (UHP) metamorphic rocks in the northern Tibetan Plateau, northwest China: International Geology Review, v. 49, p. 681–716, https://doi.org/10.2747/0020-6814.49.8.681.

Yin, A., Dang, Y., Wang, L., Jiang, W., Zhou, S., Chen, X., Gehrels, G., and McRivette, M., 2008a, Cenozoic tectonic evolution of Qaidam Basin and its surrounding regions (Part 1): The southern Qilian Shan–Nan Shan thrust belt and the northern Qaidam Basin: Geological Society of America Bulletin, v. 120, no. 7–8, p. 813–846, https://doi.org/10.1130/B26180.1.

Yin, A., Dang, Y., Zhang, M., Chen, X., and McRivette, M., 2008b, Cenozoic tectonic evolution of the Qaidam Basin and its surrounding regions (Part 3): Structural geology, sedimentation, and regional tectonic reconstruction: Geological Society of America Bulletin, v. 120, p. 847–876, https://doi.org/10.1130/B26232.1.

Yu, L., Xiao, A., Wu, L., Tian, Y., Rittner, M., Lou, Q., and Pan, X., 2017, Provenance evolution of the Jurassic northern Qaidam Basin (West China) and its geological implications: Evidence from detrital zircon geochronology: International Journal of Earth Sciences, v. 106, p. 2713–2726, https://doi.org/10.1007/s00531-017-1455-z.

Yuan, H.L., Gao, S., Liu, X.M., Li, H.M., Gunther, D., and Wu, F.Y., 2004, Precise U-Pb age and trace element determinations of zircon by laser ablation–inductively coupled plasma mass spectrometry: Geostandards and Geoanalytical Research, v. 28, p. 353–370, https://doi.org/10.1111/j.1751-908X.2004.tb00755.x.

Yue, Y., and Liou, J.G., 1999, Two-stage evolution model for the Altyn Tagh fault, China: Geology, v. 27, no. 3, p. 227–230, https://doi.org/10.1130/0091-7613(1999)027<0227:TSEMFT>2.3.CO;2.

Yue, Y., Ritts, B., and Graham, S., 2001, Initiation and long-term slip history of the Altyn Tagh fault: International Geology Review, v. 43, no. 12, p. 1087–1093, https://doi.org/10.1080/00206810109465062.

Zhang, T., Han, W., Fang, X., Zhang, W., Song, C., and Yan, M., 2016, Intensified tectonic deformation and uplift of the Altyn Tagh range recorded by rock magnetism and growth strata studies of the western Qaidam Basin, NE Tibetan Plateau: Global and Planetary Change, v. 137, p. 54–68, https://doi.org/10.1016/j.gloplacha.2015.12.017.

Zhang, T., Fang, X., Wang, Y., Song, C., Zhang, W., Yan, M., Han, W., and Zhang, D., 2018, Late Cenozoic tectonic activity of the Altyn Tagh range: Constraints from sedimentary records from the western Qaidam Basin, NE Tibetan Plateau: Tectonophysics, v. 737, p. 40–56, https://doi.org/10.1016/j.tecto.2018.04.021.

Zhong, J.H., Wen, Z.F., Guo, Z.Q., Wang, H.Q., and Gao, J.B., 2004, Paleogene and early Neogene lacustrine reefs in the western Qaidam Basin, China: Acta Geologica Sinica, v. 78, p. 736–743.

Zhu, L., Wang, C., Zheng, H., Xiang, F., Yi, H., and Liu, D., 2006, Tectonic and sedimentary evolution of basins in the northeast of Qinghai-Tibet Plateau and their implication for the northward growth of the plateau: Palaeogeography, Palaeoclimatology, Palaeoecology, v. 241, no. 1, p. 49–60, https://doi.org/10.1016/j.palaeo.2006.06.019.

Zhuang, G., Hourigan, J., Ritts, B., and Kent-Corson, M., 2011, Cenozoic multiple-phase tectonic evolution of the northern Tibetan Plateau: Constraints from sedimentary records from Qaidam Basin, Hexi Corridor, and Subei Basin, northwest China: American Journal of Science, v. 311, p. 116–152, https://doi.org/10.2475/02.2011.02.

Zhuang, G., Najman, Y., Guillot, S., Roddaz, M., Antoine, P.O., Métais, G., Carter, A., Marivaux, L., and Solangi, S.H., 2015, Constraints on the collision and the pre-collision tectonic configuration between India and Asia from detrital geochronology, thermochronology, and geochemistry studies in the lower Indus Basin, Pakistan: Earth and Planetary Science Letters, v. 432, no. 6, p. 363–373, https://doi.org/10.1016/j.epsl.2015.10.026.

Zhuang, G., Johnstone, S.A., Hourigan, J., Ritts, B., Robinson, A., and Sobel, E.R., 2018, Understanding the geologic evolution of northern Tibetan Plateau with multiple thermochronometers: Gondwana Research, v. 58, p. 195–210, https://doi.org/10.1016/j.gr.2018.02.014.

MANUSCRIPT RECEIVED 3 AUGUST 2018
REVISED MANUSCRIPT RECEIVED 19 OCTOBER 2018
MANUSCRIPT ACCEPTED 4 DECEMBER 2018